REPORT DOCUMENTATION PAGE	Form Approved OMB NO. 0704-0188

Public Reporting burden for this collection of information is estimated to average 1 hour per response, including the time for reviewing instructions, searching existing data sources, gathering and maintaining the data needed, and completing and reviewing the collection of information. Send comment regarding this burden estimates or any other aspect of this collection of information, including suggestions for reducing this burden, to Washington Headquarters Services, Directorate for information Operations and Reports, 1215 Jefferson Davis Highway, Suite 1204, Arlington, VA 22202-4302, and to the Office of Management and Budget, Paperwork Reduction Project (0704-0188,) Washington, DC 20503.

1. AGENCY USE ONLY (Leave Blank)	2. REPORT DATE	3. REPORT TYPE AND DATES COVERED Final Report 01 Jun 98 - 31 May 04

4. TITLE AND SUBTITLE ARO MURI BOWER "Understanding Olfaction: From Detection to Classification"	5. FUNDING NUMBERS G: DAAG55-98-1-0266
6. AUTHOR(S) Dr. James M. Bower, Dr. Linda Buck, Dr. William Goddard III, Dr. Denise Wilson, Dr. Nathan S. Lewis, Dr. Noam Sobel, and Dr. Gordon Shepherd	
7. PERFORMING ORGANIZATION NAME(S) AND ADDRESS(ES) California Institute of Technology 1200 E. California Blvd, M/C 127-72 Pasadena, CA 91125	8. PERFORMING ORGANIZATION REPORT NUMBER 65472
9. SPONSORING / MONITORING AGENCY NAME(S) AND ADDRESS(ES) U. S. Army Research Office P.O. Box 12211 Research Triangle Park, NC 27709-2211	10. SPONSORING / MONITORING AGENCY REPORT NUMBER 38574.25-LS-MUR

11. SUPPLEMENTARY NOTES

The views, opinions and/or findings contained in this report are those of the author(s) and should not be construed as an official Department of the Army position, policy or decision, unless so designated by other documentation.

12 a. DISTRIBUTION / AVAILABILITY STATEMENT	12 b. DISTRIBUTION CODE
Approved for public release; distribution unlimited.	

13. ABSTRACT (Maximum 200 words)

The overall objective of this research project is to support a multidisciplinary approach to understanding the function of the mammalian olfactory system across many different levels of scale. The members of the MURI collaboration represent disciplines ranging from computational chemistry, to molecular and cellular biology, to systems and computational neuroscience. Working together the objective is to shed light on structure/function relationships from the level of single olfactory receptor molecules to the function of neural circuits in olfactory regions of the mammalian brain, to olfactory related perception and cognition. In addition, the inclusion of faculty with chemical sensing and engineering expertise will allow information gleaned from biological olfactory systems to be applied to the construciton of more sophisticated devices for detecting chemicals in the environment.

14. SUBJECT TERMS	15. NUMBER OF PAGES 60
	16. PRICE CODE

17. SECURITY CLASSIFICATION OR REPORT	18. SECURITY CLASSIFICATION ON THIS PAGE	19. SECURITY CLASSIFICATION OF ABSTRACT	20. LIMITATION OF ABSTRACT
UNCLASSIFIED	**UNCLASSIFIED**	**UNCLASSIFIED**	**UL**

1) Personnel supported over course of the entire project.

Dr. Nathan S. Lewis
Brian Sisk, graduate student
Ting Gao, postdoctoral fellow
Shawn Briglin, graduate student

Dr. William Goddard III
Dr. Spencer Hall, graduate student
Dr. Rene Trabanino, , graduate student
Dr. Wely Florinao, Senior Scientist
Dr. Mario Blanco, Senior Scientist

Dr. Gordon Shepherd
Dr. Michael Hines, Research Scientist
Dr. Perry Miller, Professor
Dr. Prakash Nadkarni, Assoc. Professor
Dr. Wei Chen, postdoctoral fellow (Shanghai); Assist. Prof. (Yale)
Dr. Minghong Ma, postdoctoral fellow (Columbia) Assist. Prof., U. Pennsylvania
Dr. Andrew Davison, postdoctoral fellow (Cambridge, U.K.)
Dr. Fuqiang Xu, postdoctoral fellow (China); Assoc. Res. Sci.
Dr. Chiquito Crasto, postdoctoral fellow (India)
Dr. Zhishang Zhou, postdoctoral fellow (China)
Dr. Michele Migliore, Visiting Scientist (Italy)
Dr. Shaoquin Zeng, postdoctoral fellow (China)
Dr Fan Jia, postdoctoral fellow (China)
Peter Bail, U Conn undergraduate

Dr. James M. Bower
(Dr.) Michael Vanier, graduate student
(Dr.) Alfredo Fontinani, graduate student
(Dr.) Chris Chee, graduate student
Dr. Xiaoshu Wang, postdoctoral fellow
Dr. Yoshi Kubota, postdoctoral fellow
(Dr.) Alex Protopapas, graduate student
(Dr.) Sharon Crook, graduate student

Dr. Linda Buck
Dr. Bettina Malnic, postdoctoral fellow
Dr. Mehran Sam, postdoctoral fellow

Dr. Noam Sobel
Natasha Young, research assistant
Brad Johnson, graduate student

2) List of relevant Manuscripts published during the project.

Dr. Nathan S. Lewis:

Michael C. Burl, Brian C. Sisk, Thomas P. Vaid, and **Nathan S. Lewis**, "Classification Performance of Carbon Black-Polymer Composite Vapor Detector Arrays As a Function of Array Size and Detector and Composition," *Sens. & Act.*, **2002**, *Vol 87*, pp.130-149.

Eric S. Tillman, Michael Koscho, Robert H. Grubbs, and **Nathan S. Lewis**, "Enhanced Sensitivity To and Classification of Volatile Fatty Acids Using Arrays of Linear Poly(ethylenimine)-Carbon Black Composite Vapor Detectors," *Anal. Chem,* **2003,** *Vol 75*, pp. 1748-1753.

Alan R. Hopkins and **Nathan S. Lewis**, "Detection and Classification Characteristics of Arrays of Carbon Black/Organic Polymer Composite Chemiresistive Vapor Detectors for the Nerve Agent Simulants Dimethylmethylphosphonate and Diisopropylmethylphosponate" *Chem. & Bio. Sens. III,* Patrick J. Gardner, Ed. **2002**, *Vol. 4722*, pp. 86-97.

Shawn M. Briglin, Michael C. Burl, Michael S. Freund, Brian C. Sisk, Phillip Tokumaru, and **Nathan S. Lewis**, "Array-based Carbon Black-polymer Composite Vapor Detectors for Detection of DNT in Environments of Complex Analyte Mixtures," *Detection and Remediation Technologies for Mines and Minelike Targets VII*, J. Thomas Broach; Russell S. Harmon; Gerald J. Dobeck; Eds, **2002**, *Proc. SPIE Vol.4742.*

Brian C. Sisk and **Nathan S. Lewis**, "Estimation of Chemical and Physical Charactersistics of Analyte Vapors Through Analysis of the Response Data of Arrays of Polymer-Carbon Black Composite Vapor Detectors," *Sens. & Act., B*, **2003,** *Vol. 96*, pp. 268-282.

Eric S. Tillman and **Nathan S. Lewis**, "Mechanism of Enhanced Sensitivity of Linear Poly(ethylenimine)-Carbon Black Composite Detectors to Carboxylic Acid Vapors", *Sens. & Act., B*, **2003**, *Vol. 96*, pp. 329 - 342.

Shawn M. Briglin, Michael S. Freund, Brian C. Sisk, **Nathan S. Lewis**. "Array Based Carbon Black-Polymer Composite Vapor Detectors for Detection of DNT in Environments Containing Complex Analyte Mixtures" *Mat. Res. Soc. Symp. Proc.*, **2002** *Vol. 700.*

Keith J. Albert, **Nathan S. Lewis**, Caroline L. Schauer, Gregory A. Sotzing, Shannon E. Stitzel, Thomas P. Vaid, and David R. Walt, "Cross-Reactive Chemical Sensor Arrays", *Chem. Rev.*, **2000**,*100*, 2595-2626.

Gregory A. Sotzing, Jennifer N. Phend, Robert H. Grubbs, and **Nathan S. Lewis**, "Highly Sensitive Detection and Discrimination of Biogenic Amines Utilizing Arrays of Polyaniline/Carbon Black Composite Vapor Dectectors", *Chem. Mater.*, **2000**, *12*, 593-595.

Erik J. Severin, Brett J. Doleman, and **Nathan S. Lewis**, "An Investigation of the Concentration Dependence and Response to Analyte Mixtures of Carbon Black/Insulating Organic Polymer Composite Vapor Detectors" , *Anal. Chem,* **2000**, *72*, 658-688.

Greg A. Sotzing, Shawn M. Briglin, Robert H. Grubbs, and **Nathan S. Lewis**, "Preparation and Properties of Vapor Detector Arrays Formed From Poly(3,4-ethylenedioxy)thiophene-poly(styrene sulfonate)/Insulating Polymer Composites", *Anal. Chem* , **2000**, *72*, 3181-3190.

Brett J. Doleman and **Nathan S. Lewis**, "Comparison of Odor Detection Thresholds and Odor Discriminablities of a Conducting Polymer Composite Electronic Nose vs Mammalian Olfaction", *Sens. & Act., B,*, **2001**, *72 (1),* 41-50.

Adam J. Matzger, Carolyn E. Lawrence, Robert H. Grubbs, and **Nathan S. Lewis**, "Combinatorial Approaches to the Synthesis of Vapor Dectector Arrays for an Electronic Nose", *J. Comb. Chem.,* **2000**, *2*, 301-304.

Mike Burl, Brett J. Doleman, Amanda Schaffer, and **Nathan Lewis**, "Assessing the Ability to Predict Human Percepts of Odor Quality from the Detector Responses of a Conducting Polymer Composite-Based Electronic Nose," *Sens. & Act., B*, **2001**, *72 (2)*, 149-159.

Thomas P. Vaid, Michael C. Burl, and **Nathan S. Lewis**, "Comparison of the Performances of Different Discriminant Algorithms in Analyte Discrimination Tasks Using an Array of Carbon Black-Polymer Composite Vapor Detectors," *Anal. Chem,* **2001**, *73 (2),* 321-331.

Alan Hopkins and **Nathan S. Lewis**, "Detection and Classification Characteristics of Arrays of Carbon Black/Organic Polymer Composite Chemiresistive Vapor Detectors for the Nerve Agent Simulant Dimethylmethylphosphonate and Diisopropylmethylphosponate," *Anal. Chem,* **2001**, *73 (5),* 884-892

Shawn M. Briglin, Michael Freund, Phil Tokumaru, and **Nathan S. Lewis**, "Exploitation of Spatiotemporal Information and Geometric Optimization of Signal/Noise Performance Using Arrays of Carbon Black/Polymer Composite Vapor Detectors" *Anal. Chem* , **2002**, *82 (1),* 54-74.

Margaret A. Ryan and **Nathan S. Lewis**, "Low Power, Lightweight Vapor Sensing Using Arrays of Conducting Polymer Composite Chemically-Sensitive Resistors," *Enantiomer,* **2001**. *6 (2-3),* 159-170.

Thomas P. Vaid and **Nathan S. Lewis** "The Use of 'Electronic Nose' Sensor Responses to Predict the Inhibition Activity of Alcohols on the Cytochrome p-450 Catalyzed *p*-Hydroxylation of Aniline" *Bioorg. & Med. Chem.*, **2000** *8 (4),* 795-805.

Gregory A. Sotzing, Jennifer N. Phend, Robert H. Grubbs, and **Nathan S. Lewis** "Highly Sensitive Detection and Discrimination of Biogenic Amines Utilizing Arrays of Polyaniline/Carbon Black Composite Vapor Dectectors" *Chem. Mat.*, **2000**, *12 (3),* 593+.

Greg A. Sotzing, Shawn M. Briglin, Robert H. Grubbs, and **Nathan S. Lewis** "Preparation and Properties of Vapor Detector Arrays Formed From Poly(3,4-ethylenedioxy)thiophene-poly(styrene sulfonate)/Insulating Plymer Composites" *Anal. Chem.*, **2000** *72 (14),* 3181-3190.

Brett J. Doleman and **Nathan S. Lewis** "Comparison of Odor Detection Thresholds and Odor Discriminablities of a Conducting Polymer Composite Electronic Nose vs Mammalian Olfaction" *Sens. & Act., B*, **2000** *72 (1),* 41-50.

Erik J. Severin, Robert D. Sanner, Brett J. Doleman, and **Nathan S. Lewis** "Differential Detection of Enantiomeric Gaseous Analytes Using Carbon Black-Chiral Polymer Composite, Chemically Sensitive Resistors" *Anal. Chem.* **1998**, *70,* 1440.

Brett J. Doleman, Robert D. Sanner, Erik J. Severin, Robert H, Grubbs, and **Nathan S. Lewis** "Use of Compatible Polymer Blends to Fabricate Arrays of Carbon Black-Polymer Composite Vapor Detectors" *Anal. Chem.*, **1998**, *70,* 2560.

Brett J. Doleman, Mark C. Lonergan, Erik J. Severin, Thomas P. Vaid, and **Nathan S. Lewis** "Quantitative Study of the Resolving Power of Arrays of Carbon Black-Polymer Composites in Various Vapor-Sensing Tasks", *Anal. Chem.* **1998**, *70*, 4177.

Brett J. Doleman, Erik J. Severin and **Nathan S. Lewis** "Trends in Odor Intensity for Human and Electronic Noses: Relative Roles of Odorant Vapor Pressure vs Molecularly Specific Odorant Binding", *Proc. Natl. Acad. Sci.*, **1998**, *95*, 5442.

Dr. Gordon Shepherd

Chen, W.R., Xiong, W. and **Shepherd, G.M.,** "Analysis of relations between NMDA receptors and GABA release at olfactory bulb reciprocal synapses." *Neuron,* **2000**, *25,* 625-633.

Floriano, W.B., Vaidehi, N., Goddard, W.A.III, Singer, M.S. and **Shepherd, G.M.,** "Molecular mechanisms underlying differential odor responses of a mouse olfactory receptor." *Proc. Natl. Acad. Sci.*, **2000**, *97:* 10712-10716.

Ma, M. and **Shepherd, G.M.,** "Spatial relations of odor responses monitored by Ca2+ imaging in an intact mouse olfactory epithelial preparation." *Proc. Natl. Acad. Sci.*, **2000** *97*, 12869-12874.

Crasto, C., Marenco, L., Miller, P. and **Shepherd, G.,** "Olfactory Receptor Database: a metadata-driven automated population from sources of gene and protein sequences." *Nucl. Acids Res.,* **2000**, *30,* 354-360.

Chen, W.R., Shen, G.Y., **Shepherd, G.M.,** Hines, M.L. and Midtgaard, J., "Multiple modes of action potential initiation and propagation in mitral cell primary dendrite." *J. Neurophysiol,.* **2002,** 88: 2755-2764.

Ma, M., Grosmaitre, X., Iwema, C.L., Baker, H., Greer, C.A. and **Shepherd, G.M.**, "Olfactory signal transduction in the mouse septal organ." *J. Neurosci.*, **2003**, *23,* 317-324.

Crasto, C., Marenco, L.N., Migliore, M., Mao, B., Nadkarni, P.M., Miller, P. and Shepherd, G.M., "Text mining neuroscience journal articles to populate neuroscience databases." *Neuroinformatics*, **2003**, *1,* 215-238.

Liu, N., Xu, F.Q., Marenco, L, Miller, P. and **Shepherd, G.M.,** "Informatics approaches to functional MRI odor mapping of the rodent olfactory bulb: OdorMapBuilder and OdorMapDB." *Neuroinformatics*, in press.

Xu, F.Q, Liu, N., Kida, I., Rothman, D.L., Hyder, F. and **Shepherd, G.M.** "Odor maps of aldehydes and esters revealed by fMRI in the glomerular layer of the mouse olfactory bulb." *Proc. Nat. Acad. Sci. USA*, **2003**, *100*, 11029-11034.

Chapters, Reviews

Xu, F.Q., Greer, C.A. and **Shepherd, G.M.,** "Odor maps in the olfactory bulb." *J. Comp. Neurol.*, **2000**, *422,* 489-495.

Crasto, C., Singer, M.S. and **Shepherd, G.M.**, "The olfactory receptor family album." *Genome Biology*, **2001**, (online).

Ma, M. and **Shepherd, G.M.** "Recordings from vertebrate olfactory receptor neurons: from isolated cells to intact epithelial preparations." In Methods in Chemosensory Research (Ed. Simon, S.A. and Nicolelis, M.A.L.) New York: CRC Press, **2002**, pp. 65-78.

Xu, F., Greer, C. and **Shepherd, G.M.**, "Application of fMRI in olfactory studies." In Methods in Chemosensory Research (Ed. Simon, S.A. and Nicolelis, M.A.L.) New York: CRC Press, **2002**, pp. 465-476.

Migliore, M. and **Shepherd, G.M.**, "Emerging rules for the distributions of active dendritic conductances." *Nature Neurosci. Revs.* **2002**, *3,* 362-370.

Chen, W.R. and **Shepherd, G.M.**, "Putting odor maps in sync." *Nature Neurosci.* **2002,** *5*, 505-506.

Shepherd, G.M. "Passive membrane properties of axons and dendrites." In Fundamental Neuroscience (ed. F. Bloom et al). New York: Academic Press, **2003**, pp. 115-139.

Shepherd, G.M., "Information processing in complex dendrites." In Fundamental Neuroscience (ed. F. Bloom et al). New York: Academic Press, **2003**, pp. 319-338.

Shepherd, G.M., "The single capillary and the active brain.", *Proc. Natl. Acad. Sci. USA*, **2003**, *100,* 12535-12536.

Shepherd, G.M., Crasto, C. and Singer, M.S., "Olfactory genes and flavour perception: implications for the evolution of human cuisines.", In Flavour Research at the Dawn of the Twenty-first Century. *Proc. 10th Weurman Flavour Res. Symp.* (ed. Le Quere, J.-L., and Etievant, P.X.) London: Lavoiser/Intercept, **2003**, pp.263-268.

Shepherd, G.M., "Implications of recent research on olfaction for the neural basis of flavor in humans: challenges and opportunities." In Handbook of Flavor Characterization. Sensory Analysis, Chemistry, and Physiology (ed. Deibler, K.D. and Delwiche, J.). New York: Marcel Dekker, **2004**, pp. 93-104.

Shepherd, G.M., "Passive membrane properties of axons and dendrites. In From Molecules to Networks.", An Introduction to Cellular and Molecular Neuroscience (ed. Byrne, J.H. and Roberts, J.L.). New York: Academic Press, **2004**, pp. 115-139.

Shepherd, G.M., "Information processing in complex dendrites." In From Molecules to Networks. An Introduction to Cellular and Molecular Neuroscience (ed. Byrne, J.H. and Roberts, J.L.). New York: Academic Press, **2004**, pp. 319-338.

Shepherd, G.M. "The human sense of smell: is it more important than we think?" *PLOS Biology*, **2004**, in press.

Book
Shepherd, G.M. (Ed.), "The Synaptic Organization of the Brain (Fifth Edition).", New York: *Oxford University Press*, **2004**.

Dr. James Bower:
Vanier, M, and **Bower, J.M.,** "Computational modeling of olfactory cortex." *J. Comp. Neurosci.* **2004**, submitted.

Protopapas, A. and **Bower, J.M.**, "Spike coding in pyramidal cells in the piriform cortex of rat." *J. Neurophysiol.* **2001**, 86: 1504-1510

Vanier, M. and **Bower, J.M.,** "Synaptic effects of norepinephrine in piriform cortex", **2004**, submitted.

Chee-Ruiter, C.W.J., Madany Mamloukm, A, and **Bower, J.M.**, "Mapping odor descriptors: Implications for the organization of human olfactory processing Chemical Senses.", **2004**, submitted.

Fontanini , A., and **Bower, J.M.**, "Slow and fast oscillations in olfactory cortex" *J. Neurosci.*, **2004**, submitted.

Amir Madany Mamloukm, A., Chee-Ruiter, C., Hofmann, U.G., and **Bower, J.M.**, "Mapping olfactory perception space by using multidimensional scaling and self-organizing maps." *Neurocomputing*, **2003**, *52-54,* 591-597.

Fontanini , A., Spano, P.F., and **Bower, J.M.,** "Ketamine/xylazine induced slow (<1.5 Hz) oscillations in the rat piriform (olfactory) cortex are functionally correlated with respiration", *J. Neurosci.*, **2003**, *23,* 7993-8001.

Kubota Y, **Bower JM.**, "Transient versus asymptotic dynamics of CaM kinase II: possible roles of phosphatase.", *J Comput Neurosci.*, **2003**, *Nov-Dec;11(3),* 263-79.

Protopapas, A. and **Bower, J.M.**, "Spike coding in pyramidal cells in the piriform cortex of rat." *J. Neurophysiol.* **2001**, *86,* 1504-1510.

Sobel, N., Thomason, M.E., Stappen, I, Tanner, C.M., Tetrud, J. W., **Bower, J.M.**, Sullivan, E.V., Gabrieli, D.E., "An impairment in sniffing contributes to the olfactory impariment in Parkinson's Disease.", *PNAS* **2001**, *98,* 4154-4159.

Protopapas AD, **Bower J.M.**, "Physiological characterization of layer III non-pyramidal neurons in piriform (olfactory) cortex of rat." *Brain Res.*, **2000**, *865,*1-11.

Chee-Ruiter, C.W.J., and **Bower, J.M.**, "Biological search strategies for chemical plume tracing.", *Proceedings of the EREDC Conference on Chemical and Biological Defense Research*, 1999, pp 41-47.

Kubota, Y., and **Bower, J.M.,** "Decoding time-varying calcium signals by postsynaptic biochemical networks: Computer simulations of molecular kinetics.", *Neurocomputing*, **1999**, *26,* 29-38.

Chee-Ruiter, C. and **Bower, J.M.**, "Representing Odor Quality Space: A Perceptual Framework for Olfactory Processing", in *Computational Neuroscience: trends in research*, J.M. Bower, ed., Plenum Press, NY **1998**.

Crook, S.M., Ermentrout, G.B., and **Bower, J.M.**, "Spike frequency adaptation affects the synchronization properties of networks of cortical oscillators." *Neural Computation.,* **1998,** *10,* 837-854.

Crook, S., Ermentrout, G.B., and **Bower, J.M.**, "Dendritic and synaptic effects in systems of coupled cortical oscillators." *J. Computational Neurosci.* **1998,** *5,* 315-329.

Protopapas, A., M. Vanier and **Bower, J.M.** "Simulating networks of neurons." In: Methods in Neuronal Modeling: From Synapses to Networks. C. Koch and I. Segev, editors. MIT Press, Cambridge, MA, **1998**.

Dr. Linda Buck:

Malnic B, Hirono J, Sato T and **Buck L.B.,** "Combinatorial receptor codes for odors.", *Cell,* **1999**, *96,* 713-723.

Horowitz LF, Montmayeur J, Echelard Y and **Buck L.B.,** "A genetic approach to trace neural circuits.", *Proc. Natl. Acad. Sci. USA,* **1999**, *96,* 3194-3199.

Buck L.B., "The molecular architecture of odor and pheromone sensing in mammals.", *Cell,* **2000**, *100,* 611-618.

Sam M, Vora S, Malnic B, Ma W, Novotny MV and **Buck L.B.,** "Odorants may arouse instinctive behaviours." *Nature*, **2001**, *412,* 142.

Zou Z, Horowitz LF, Montmayeur J-P, Snapper S and **Buck L.B.,** "Genetic tracing reveals a stereotyped sensory map in the olfactory cortex.", *Nature*, **2001,** *414*,173-179.

Buck L.B., "The search for odorant receptors.", *Cell*, **2004**, *116,* 117-119.

Godfrey PA, Malnic B, and **Buck L.B.,** "The mouse olfactory receptor gene family.", *Proc. Natl. Acad. Sci. USA.*, **2004**, *101,* 2156-2161.

Malnic B, Godfrey PA, and **Buck L.B.,** "The human olfactory receptor gene family." *Proc. Natl. Acad. Sci. USA.*, **2004,** *101*, 2584-2589.

Dr. Noam Sobel

Mainland, J., Bremner, E., Young, N., Johnson, B., Khan, R., Bensafi, M., **Sobel, N.** "Olfactory Plasticity: One nostril knows what the other learns.", *Nature,* **2002,** 419 802.

Anderson, K. Christoff, I. Stappen, D. Panitz, D. G. Ghahremani, G. Glover, J.D.E. Gabrieli, & **Sobel, N.** "Olfaction dissociates the neural representation of intensity and valence in humans.", *Nature Neuroscience,* **2002**, *6(2)*, 196-202.

Johnson BN, Mainland JD, **Sobel N.** "Rapid olfactory processing implicates subcortical control of an olfactomotor system.", *J Neurophysiol.*, **2003**, *90(2),* 1084-94.

3) List of relevant inventions over the course of the entire project.

US Pat. No. 6,495,892 Techniques and systems for analyte detection
US Pat. No. 6,467,333 Trace level detection of analytes using artificial olfactometry
US Pat. No. 6,455,319 Use of spatiotemporal response behavior in sensor arrays to detect analytes in fluids
US Pat. No. 6,387,329 Use of an array of polymeric sensors of varying thickness for detecting analytes in fluids
US Pat. No. 6,350,369 Method and system for determining analyte activity

4) Technology Transfer over the course of the entire project.

Some patents licensed to startup company: Cyrano Sciences, and other patents being licensed to Caltech.

Dr. Nathan S. Lewis:

Prediction of Physical Analyte Data Based on Interactions with a Chemical Vapor Detection System

Introduction

The use of Quantitative Structure-Activity Relationship (QSAR) and Quantitative Structure-Property Relationship (QSPR) techniques has allowed for the characterization of untested molecules based on similarities to a library of experimentally characterized molecules. Essentially, the QSAR/QSPR method involves the development of a prediction model that matches an array of experimental data. This model can be of effectively any quantitative nature, and many methods have been used, such as multiple linear regression, partial least squares, neural network analysis, and genetic functional analysis.

QSAR/QSPR has been particularly useful for drug discovery, for which a fast method of pre-screening drug candidates based on expected characteristics is necessary. Additionally, this technique has been used to predict fundamental properties of molecules, such as thermodynamic constants, based on their structures. However, these methods often employ semi-quantitative "features," such as the number of double bonds or benzene ring in a structure[1], or other thermodynamic data[2]. However, such data can be subjective (in the case of semi-quantitative features) or not available for all possible molecules of interest (in the case of thermodynamic data). For these reasons, a method that is based on simple, fast experimental methods may in some situations be desirable.

Recent studies have shown that the responses of polymer-based chemical vapor detectors can be modeled by thermodynamic relationships between the polymer sensor and analyte vapor.[3] This is reasonable, considering that detector responses are largely determined by the partition coefficient K, which varies for every combination of analyte and polymer.[3,4] Therefore, it is reasonable that the reverse should also be possible - that is, the responses of an array of different detectors to a library of analytes should allow for the development of a predictive model that characterizes analytes based upon their responses to a chemical detector array.

Such an attempt was made by Vaid et al., in which cytochrome-p450 activity for a series of alcohols was predicted based upon the responses of these alcohols to a detector array.[5] In this case, Genetic Functional Analysis (GFA)[6] was used to develop a predictive model relating cytochrome-p450 activity to sensor responses. GFA yielded 100 different models, which were ranked based on their lack-of-fit (LOF, equation 1).

eq 1. $LOF=LSE/(1-((c+dp)/M)^2)$

Ultimately, the equation used to model cytochrome-p450 activity for alcohols yielded a high degree of statistical significance as determined by its LOF and F-test values. Because the set was quite small, cross-validation was not performed - rather, an estimated cross-validation R^2 value was determined from the basis dataset.

Experimental

For our current work, we seek to explore whether other characteristic analyte properties may be predicted from sensor responses. We have explored bulk analyte properties (water/octanol partition coefficients (K_{ow})), size-related physical parameters (van der Waals area, volume, and radius of gyration), and energetic parameters such as solubility parameter $((\Delta H\text{-}RT)/V_m)^{1/2}$ and Hansen energies, which are decomposed from solubility parameter as shown in eq 2.:

Eq 2. $$SP = ([(Han_E)^2 + (Han_D)^2 + (Han_{HB})^2]/ V_m)^{1/2}$$

Here, Han_E, Han_D, and Han_{HB} are the Hansen electrostatic, dipole, and hydrogen bonding components of the Hildebrandt cohesive energy, respectively; SP is the solubility parameter term, and V_m is the liquid molar volume. Our research did not focus on the Hansen hydrogen bonding term because of the small number of analytes in our set that possessed non-zero values for this property. All values were acquired from the DIPPR online database.[7] Values of K_{ow} and solubility parameters were determined experimentally, while other values were derived or calculated.

An array of 40 sensors, 2 copies each of 20 different detectors, was exposed 10 times to each of 75 different analytes, which fall roughly into five classes: alcohols, halides, aromatics, hydrocarbons, and esters. Responses of each sensor to each analyte exposure were determined by calculating the fractional steady-state resistance change of each sensor, $\Delta R_{eq}/R_b$. More details regarding this sensor array and analyte set, used for other work, are described elsewhere.[8]

To form a basis for prediction models, the data were divided into a training set (consisting of 18 analytes) which was used to build the models, a validation set (consisting of 19 analytes) used to choose the best model, and a test set (consisting of 37 analytes) that was used to evaluate the model. To ensure that the test set was interpolating rather than extrapolating based on the model, any analytes that possessed either the highest or lowest values for any property considered were assigned to the training set. The other analytes were randomly assigned set membership, while assuring that each analyte class contributed roughly evenly to ensure that each class was fairly represented in each set.

Previous work, both with cytochrome-p450 activity prediction and with prediction of the properties here, was performed using GFA models that utilized a handful of sensors. However, this method has the disadvantage that a great deal of useful information may be contained in the sensors rejected, while using more sensors would slow the algorithm and almost certainly result in overtraining. For this reason, rather than choosing sensors the data was first transformed using Fisher's Linear Discriminant (FLD).[9] FLD takes as input our 40-dimensional sensor data, and transforms the data such that the greatest portion of the data which distinguishes the different analytes is contained in the first few dimensions. In this way, well over 99% of the 40-dimensional information can be contained in as few as five dimensions. This simplifies the models and reduces the risk of overtraining, while retaining nearly all of the useful information in the data. As such, linear models are used for our current work, and rather than using GFA to select what sensors to use (out of ${}_{40}C_5$=658008 possible combinations), we simply choose the most significant X FLD dimensions, where X is allowed to vary between 3 and 11, after which the FLD components contain virtually no information (less than 1% of that contained in the first component). The value X chosen is that

which minimizes the root mean squared error (RMSE) of the validation set. This process is repeated for each of the properties investigated, with a single model chosen for each property, and these models are then used to predict the properties of those analytes in the test set.

Results

As might be expected, some properties are more easily related to vapor/polymer interactions, others less. Results of this analysis are shown in Table 1. FCs refers to the number of FLD components used for the model, and RMSE/range refers to a ratio of the RMSE of the test set data to the range of the data. R^2, slope, and int/range of the test set all refer to statistics derived from a correlation of actual and predicted properties from the test set data. Int/Range refers to the fit intercept divided by the range of the data.

Property	# FCs	RMSE/Range	R^2, test	Slope	Int./Range
K_{ow}	**5**	**0.0865**	0.864	1.001	7.1×10^{-4}
van der Waals Volume	**11**	**0.1583**	0.607	0.7750	0.2489
van der Waals Area	**10**	**0.1607**	0.548	0.9180	0.1012
Radius of Gyration	**10**	**0.1944**	0.352	0.6941	0.3123
Solubility Parameter	**9**	**0.1116**	0.869	0.8897	0.1135
Hansen Dipole	**11**	**0.1894**	0.513	0.8037	0.6141
Hansen Electrostatic	**5**	**0.2473**	0.626	1.011	-0.1589

Table 1. Analysis of LinearModels Developed for Prediction of Thermodynamic/Physical Parameters

A wide disparity exists in these results, with K_{ow} and SP predicting very well, radius of gyration predicting very poorly, and the other results in between. Van der Waals area and volume predicted well save for an outlier which skewed the results. Note that this method is a fully blind experiment as well, with the algorithm having never been trained on the analytes whose properties it was asked to predict, and the test set was twice as large as the training set. Using larger datasets, or a leave-one-out cross validation method,[9] would likely allow for greater success.

References:

1. Fitch, WL, McGregor, M, Katritzky, AR, Lomaka, A, Petrukhin, R, Karelson, M, *J. Chem. Inf. Comput. Sci.* **2002**, *42*, 830-840.
2. Xing, L, Glen, RC, *J. Chem. Inf. Comput. Sci.* **2002**, *42*, 796-805.
3. Hierlemann, A, Zellers, ET, Ricco, AJ, *Anal. Chem.* **2001**, *73*, 3458-3466.
4. Severin, EJ, Doleman, BJ, Lewis, NS, Anal. Chem. **2000**, *72*, 658-668.
5. Vaid, TP, Lewis, NS, *Bioorg. Med. Chem.* **2000**, *8*, 795-805.
6. Rogers, D, Hopfinger, AJ, *J. Chem. Inf. Comput. Sci.* **1994**, *34*, 854-866.
7. DIPPR Chemical Database, "http://dippr.byu.edu/public/chemsearch.asp", Brigham Young University DIPPR Thermophysical Properties Laboratory.
8. Duda RO, Hart PE, *Pattern Classification and Scene Analysis.* New York: John Wiley and Sons, **1973**.
9. Sisk, BC, Lewis, NL, *Sens. Actuators B – Chem.*, **2003**, *96*, 268-282.

Dr. William A. Goddard III:

Section I

Response of Electronic Noses and the Analyte Partition Coefficient
S.T. Lin, M. Blanco, W. A. Goddard III
Materials and Process Simulation Center (MSC), Caltech

1.0 Introduction

It is known that for each polymer film sensor the response (increase in resistivity ΔR) is only a function of the swelling volume of the film.[1] In other words, the change of conductivity is the same as long as the same volume change ΔV in the polymer film is caused, regardless of the nature of the chemical molecule.

$$\frac{\Delta R}{R} = f_p(\frac{\Delta V}{V}) \tag{1}$$

This experimental evidence indicates that one could predict the response of such electronic nose if the partition coefficient of the analyte in the polymer film and the molar volume of the analyte are known. Assuming the swelling of the polymer is ideal, the relative volume change of the polymer film can be determined from

$$\frac{\Delta V}{V} = K_H c_a^{vap} \underline{V}_a^L = K_H \frac{P_a^{vap} \underline{V}_a^L}{RT}(\frac{P_a}{P_a^{vap}}) \tag{2}$$

where P_a is the partial pressure of the analyte, P_a^{vap} is the vapor pressure, $\underline{V}_a^L$ is the molar volume of the analyte in the pure liquid state, and the partition coefficient K_H is defined as the ratio of analyte concentration in the vapor phase c_a^{vap} versus the polymer matrix $c_a^{polymer}$ in the limit of zero analyte partial pressure, i.e.,

$$K_H = \lim_{c_a^{vap} \to 0} \frac{c_a^{polymer}}{c_a^{vap}} \tag{3}$$

1.1 Perturbation Method for Calculation of Partition Coefficient

The partition of analyte molecules in the gas and polymer is determined by the equality of the chemical potential in the two phases, i.e., $\mu_a^{vap}(T,P,c_a^{vap}) = \mu_a^{polymer}(T,P,c_a^{polymer})$. The Widom's particle insertion method[2] is one of the commonly used techniques for determining chemical potentials. For a system containing N_a analyte molecules and N_p polymer molecules, the μ of analyte can be expressed in terms of the interaction energy, Ψ, between a ghost analyte and the analyte-polymer mixture

$$\mu_a(N_a,N_p,P,T) = kT\ln\frac{q_a}{<\rho_a>_{N_a+N_p}\Lambda_1^3} - kT\ln<\frac{V}{<V>_{N_a+N_p}}\exp(-\hat{a}\Psi)>_{N_a+N_p} \tag{4}$$

where V is the volume of the polymer-analyte mixture, q_a and ρ_a are the internal partition function and number density of the analyte, N_a and N_p are the number of analyte and

polymer molecules, Ψ is the energy differences between the systems with N_a+1 analyte molecules and with N_a molecules, i.e., $\Psi = U(N_a + 1, N_p) - U(N_a, N_p)$, and <> indicates ensemble averages. Assuming the analyte is ideal in the gas phase, i.e., $\mu_a^{IG}(T,P) = -kT \ln \frac{q_1}{\rho^{IG} \Lambda_1^{\,3}}$, the partition coefficient can be calculated from the ensemble average of Ψ

$$\ln K_H = \ln < \frac{V}{< V >_{N_a+N_p}} \exp(-\hat{a}\Psi) >_{N_a+N_p} \tag{5}$$

Molecular dynamics simulation is a useful tool for determining K_H based on the Widom's formulation (eq. 5). Since preferred interactions, i.e. negative ψ, is rarely observed in high density simulations, a common practice to improve the ensemble average is to gradually "turn on" the interactions between the ghost analyte molecule and the polymer, i.e.,

$$\ln K_H = \sum_{j=0}^{M-1} \ln < \frac{V}{< V >_{N_1+N_2+\ddot{e}_j}} \exp(-\hat{a}\Psi_{\ddot{e}_j}) >_{N_1+N_2+\ddot{e}_j} \tag{6}$$

where λ is a perturbation parameter that varies from 0 at j=0 to 1 at j=M, and the perturbed interaction Ψ_{λ_j} is

$$\Psi_{\lambda_j} = U(N_1 + \ddot{e}_{j+1}, N_2) - U(N_1 + \ddot{e}_j, N_2) = (\ddot{e}_{j+1} - \ddot{e}_j)\Delta U_{a-p} \tag{7}$$

with ΔU_{a-p} being the interaction between the ghost (or perturbed) analyte molecule and the other molecules in the system, i.e.,

$$\Delta U_{a-p} = \sum_{i=1}^{N_1} \sum_{j=1}^{N_2} (U_{ij}^{VDW} + U_{ij}^{COUL}) \tag{8}$$

where N_1 is the total number of atoms in the ghost analyte and N_2 is the atoms of all other atoms in the system. U_{ij}^{VDW} and U_{ij}^{COUL} are the normal van der Waals and coulomb interactions between atoms i and j. This is referred as the Multiple Step Thermodynamic Perturbation (MSTP) method.[3] The MSTP method has also been implemented in molecular dynamics methods.[4]

2.0 Implementation and Test of the Multiple Step Thermodynamic Perturbation method

The MSTP method has been implemented in LAMMPS, a parallel molecular dynamics simulations code developed in the Sandia National Lab.[5] The following analytical equation is used to determine the values of the perturbation parameter λ at any simulation step n_i

$$\ddot{e}_i = \ddot{e}_0 \exp\left[-\left(\frac{n_i - n_0}{n_f - n_0}\right) + b\left(\frac{n_i - n_0}{n_f - n_0}\right)^3 \right] \tag{9}$$

where n_0 and n_f are the initial and final simulation step number, and the constant b is determined by the initial and final values of λ, i.e, $b = 1 + \ln \frac{\ddot{e}_f}{\ddot{e}_0}$. Equation 9 gives a

linear dependence of λ with n when λ is close to 1 and exponential dependence when λ is close to 0. To validate the LAMMPS implementation of the MSTP method, we determine the free energy of a Lennard-Jones liquid at reduced temperature of 0.9 and reduced density of 0.85. Figure 1 shows the instantaneous and integrated values of the free energy of growing (λ varies from 0 to 1) and removing (λ varies from 1 to 0) a particle in the system. The results -2.22 and 2.10 are in excellent agreement with the theoretical value of ±2.14.

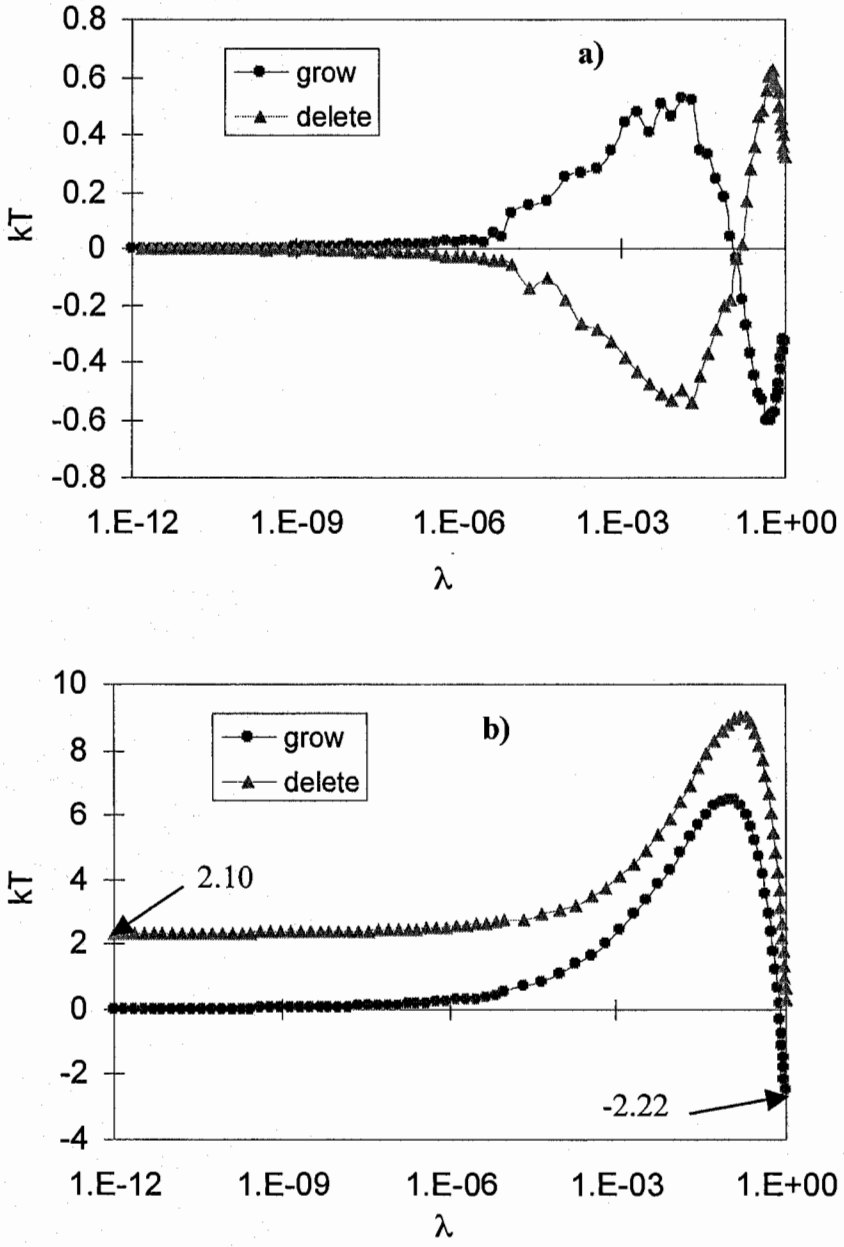

Figure 1. The instantaneous (a) and integrated (b) values of free energy change for a Lennard-Jones liquid at reduced temperature of 0.9 and reduced density of 0.85.

The free energy changes for both growing (λ varies from 0 to 1) and reducing (λ varies from 1 to 0) a ghost particle are shown.

2.1 Application to Electronic Nose Sensors: Partition Coefficient of Analytes in Polymer Poly-Ethylene Oxide (PEO)

We aim at predicting the response of electronic nose polymeric sensors to a wide variety of analytes. Experimental data for various polymers, including PEO is available.[1] To study the partition coefficient K_H of analyte in polymers, we performed MD simulations on 6 analytes for which experimental data is available (dichloromethane CH_2Cl_2, chloroform $CHCl_3$, dibromomethane CH_2Br_2, bromoform $CHBr_3$, benzene C_6H_6, and hexafluorobenzene C_6F_6) in PEO. Figure 2 shows the typical change in free energy as a function of λ for CH_2Cl_2. (similar curves are observed for other analytes.) The free energy curve for the growing process starts at negative values, at small values of λ, and turns over to positive values, at large λ. This indicates a competition between the favorable interactions and unfavorable repulsive interactions at different values of λ. At small λ values the interaction between the analyte and polymer is weak. The fractional analyte can occupy the free volume of the polymer without changing the polymer conformation. The increase of λ improves the attractive interactions between the analyte and polymer, leading to negative values of the free energy. However, at large values of λ, the increasing repulsive interactions become more significant. In other words, the polymer has to change its conformation to create more volume for the growing analyte. Therefore, a positive free energy is observed at large λ values.

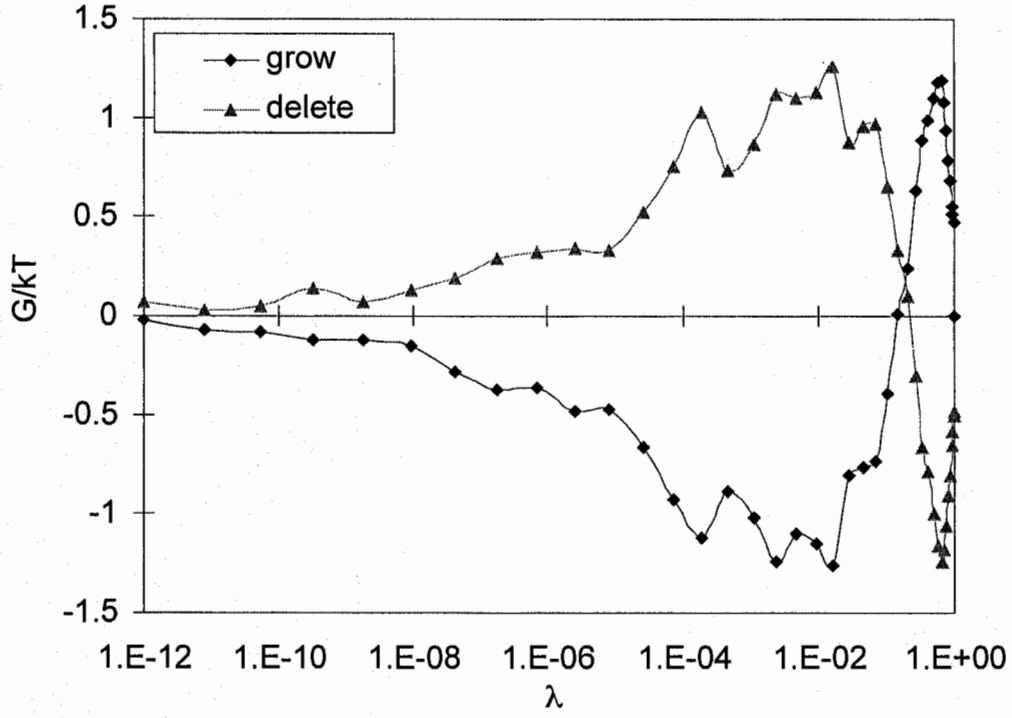

Figure 2. Instantaneous values of free energy for dichloromethane in PEO at different λ.

The predicted partition coefficients for all six analytes are compared with experiment in Table 1. A qualitative agreement between experimental measurements is obtained. Discrepancies may be the result of insufficient sampling, which is known to be crucial for polymer simulations. At the same time the measurements are subject to experimental uncertainty. For example, ellipsometry measurements are typically higher, by factors of 3, than the results of the quartz-crystal microbalance (QCM) quoted here.

Table 1. Comparison of the predicted and experimental values of partition coefficient $\ln K_H$ for 6 analytes in PEO at 300 K.

analyte	$\ln K_H$(expt)	$\ln K_H$(calc)
CH_2Cl_2	1.91	4.85
$CHCl_3$	3.34	6.44
CH_2Br_2	4.47	6.36
$CHBr_3$	6.42	7.39
C_6H_6	2.58	5.89
C_6F_6	0.80	-2.01

To examine the importance of sampling, we have also performed two tests: (1) increase the number of simulation cycles and (2) increase the number of perturbed analyte molecules in the system. Table 3 compares the results using either one or three cycles, i.e., repeating the change of λ from 0 to 1 and back to 0 one or three times. It is found that the increase of simulation cycles uniformly decreases the values and improves the prediction of $\ln K_H$. Therefore, the increase of cycles can reduce the bias towards poor polymer-analyte interactions. It seems then that the polymer undergoes a non-reversible hysteresis that requires a few cycles to equilibrate.

Table 2. The predicted partition coefficient $\ln K_H$ with multiple MSTP cycles.

analyte	$\ln K_H$(expt)	$\ln K_H$(calc, 1 cycle)	$\ln K_H$(calc, 3 cycles)
CH_2Cl_2	1.91	4.85	0.96
CH_2Br_2	4.47	6.36	3.83
$CHBr_3$	6.42	7.39	4.75

A second test is performed on the CH_2Cl_2-PEO system using 1, 5, and 10 analyte molecules. The multiple analytes behave as individual probes sampling different regimes of the polymer. Table 3 compares the predictions of $\ln K_H$ using different number of analyte probes. It is found that having multiple analytes in the system also help improve the sampling. This approach is much more efficient than the previous multiple cycle approach and is preferred for the future study of the analyte partition in polymer sensors.

Table 3. Comparison Effects of samplings and number of analytes in the simulation.

analyte	CH_2Cl_2
$\ln K_H$(expt)	1.91
$\ln K_H$(1 CH_2Cl_2, 1 cycle)	4.85
$\ln K_H$(1 CH_2Cl_2, 3 cycles)	0.96
$\ln K_H$(5 CH_2Cl_2, 1 cycle)	0.80
$\ln K_H$(10 CH_2Cl_2, 1 cycle)	1.12

Conclusions

In this work we have used the thermodynamic perturbation method to determine the partition coefficient, the key component of determining the polymer sensor response, for six analytes in poly(ethylene oxide). We have implemented the multiple step thermodynamic perturbation (MSTP) algorithm in a parallel molecular dynamic simulation program LAMMPS. In MSTP, we adjust the polymer-analyte interaction through a perturbation parameter λ whose value varies between 0 and 1. Integrating the free energy change of the polymer-analyte composition from λ=0 to 1 gives the partition coefficient. Good agreement with experimental measurements is found when enough samplings are considered. The MSTP method is a practical and useful tool for studying the dependence of polymer sensor repose on different analyte and/or polymer chemical structures, humidity, temperature, and plasticitizers.

References:

1 E. J. Severin and N. S. Lewis, Analytical Chemistry **72** (9), 2008 (2000).

2 B. Widom, J. Chem. Phys. **39** (11), 2808 (1963).

3 D. Frenkel and B. Smit, *Understanding Molecular Simulation From Algorithms to Applications*. (Academic press, New York, 2002).

4 D. A. P. D.A. Case, J.W. Caldwell, T.E. Cheatham III, J. Wang, W.S. Ross, C.L., T. A. D. Simmerling, K.M. Merz, R.V. Stanton, A.L. Cheng, J.J. Vincent, M. Crowley,, H. G. V. Tsui, R.J. Radmer, Y. Duan, J. Pitera, I. Massova, G.L. Seibel, U.C., and P. K. W. a. P. A. K. Singh, AMBER (University of California, San Francisco, 2002).

5 S. Plimpton, LAMMPS - Large-scale Atomic/Molecular Massively Parallel Simulator (Sandia National Laboratories, Albuquerque, 2001).

Dr. William A. Goddard III:

Section II

Hildebrand and Hansen Solubility Parameters from Molecular Dynamics with Applications to Electronic Nose Polymer Sensors

M. Blanco, and W. A. Goddard III
Materials and Process Simulation Center, California Institute of Technology

1.0 Introduction

In 1936 Joel H. Hildebrand proposed[1] a simple definition for a "solubility parameter" that would provide a systemic description of the miscibility behavior of solvents and which subsequently has found multiple uses in chemistry. This solubility parameter δ is defined as square root of the cohesive energy density, the heat of vaporization divided by the molar volume. Hansen[2] proposed an extension of the Hildebrand parameter method to estimate the relative miscibility of polar and hydrogen bonding systems. In Hansen's approach the Hildebrand solubility parameter is split into three components, polar, dispersion, and hydrogen bonding, thus the name 3D solubility parameters. The three components are empirically fitted to define the miscibility characteristics of the solvent. Solvents with similar Hansen solubilities are miscible in most proportions; dissimilar values yield limited solubilities. Hildebrand and Hansen solubility parameters are useful for selecting solvents and additives in formulations, for the blending of polymers, for the control of kinetics and monomer sequence distributions in copolymers, and for the proper selection of time-release formulations in the delivery of pharmaceuticals. The first principles predictions of Hildebrand solubility parameters is of great practical value in chemical formulation work. Unfortunately, it has been difficult to obtain sufficient experimental information to define all of the parameters needed in developing new formulations.

Consequently, several groups have attempted to develop general computational tools to estimate Hildebrand and Hansen solubility parameters. Choi and Kavasallis first used atomistic simulations to estimate the solubility parameters of a class of alkyl phenol ethoxylates[3] and later applied it to the estimation of 3D Hansen solubility parameters[4]. A related method has been applied to the estimation of the solubility parameters for distributions of asphaltenes, resins, and oils from crude oils and related materials.[5] The accuracy of these methods depends on the correct building of the bulk structure as well as on the molecular force field parameters used in the calculations. Numerous approaches for building amorphous polymers and liquids have been published.[6-11] Some of these methods involve growing the polymer chains at a fixed experimental density using rotational isomeric state (RIS) statistics in combination with a scaled down atomic radius followed by potential energy minimization with periodic boundary conditions. Other methods simulate a "polymerization" process to grow the chain in a fixed density. A computationally expensive protocol involving chain growth at low density followed by a pressure-induced compression with molecular dynamics has also been reported.[12] Most of these methods have been successfully used to generate amorphous structures and have correctly predicted the solubility parameters of a few polymers.

Here we report on a multi-sample molecular dynamics method which provides a feasible tool for

estimating Hildebrand and Hansen solubility parameters *without* the need for experimental data. The molecular dynamics method developed in this work is particularly useful in rapidly generating structures of polymers with large monomer units containing rings or other complex groups. The finite number of densification and equilibration steps regardless of polymer size allows for a gradual packing adjustment and the uniform redistribution of stresses among the polymer chains. This new method was validated by several studies where solubility parameter calculations were successfully correlated with experimental measurements.

For improved accuracy, the new method employs quantum mechanical charges of single molecules. However, semi-empirical methods for charge assignment, such as QEq,[13] give somewhat comparable results for molecules containing first group elements. The most significant approximation comes from the use of a generic force field for the estimation of dispersion and hydrogen bonding. Approximations not withstanding, calculated Hildebrand parameters compare well with experimental values for a series of solvents and monomer molecules. As an application example, we illustrate the use of these values in the design of polymer sensors for an electronic nose.

1.1 Method

The Hildebrand solubility parameter for a pure liquid substance is defined as the square root of the cohesive energy density.

$$\delta = [\,(\Delta H_v - RT)/V_m\,]^{1/2} \qquad (1)$$

ΔH_v is the heat of vaporization and V_m the molar volume. Typical units are

$$1 \text{ hildebrand} = 1 \text{ cal}^{1/2}\text{cm}^{-3/2} = 0.48888 \text{ x MPa}^{1/2} = 2.4542 \text{ x}10^{-2} \text{ (Kcal/mol)}^{1/2} \text{ A}^{-3/2} \quad (1a)$$

Hansen[2] proposed an extension of the Hildebrand parameter to estimate the relative miscibility of polar and hydrogen bonding systems

$$\delta^2 = \delta_d^{\,2} + \delta_p^{\,2} + \delta_h^{\,2} \qquad (2)$$

where δ_d, δ_p and δ_h are the dispersion, electrostatic, and hydrogen bond components of δ, respectively. For molecules whose heats of vaporization can be measured or calculated, one can easily determine the value of δ. The Hansen solubility parameters in Equation (2) are determined empirically based on multiple experimental solubility observations. However, for polymers the Hansen parameters are assigned to the parameters of the solvent causing the maximum swelling in a series of polymer swelling experiments. Thus, the two quantities represented by Equation (1) and (2) are expected to be similar but not identical, because the Hildebrand parameters are not always determined from heats of vaporization, particularly for substances with high boiling points. For polymers, a variety of other experimental methods are also used[14] leading to a wide range of values for any given polymer.

We report here the Cohesive Energy Density (CED) protocol based on Molecular Dynamics (MD) calculations under periodic boundary conditions (PBC) to determine an ensemble of

temperature and pressure equilibrated structures from which we can extract properties of the liquid, inlcuding the Hansen and Hildebrand solubilities of solvents and polymers. CED leads to sytematic estimates of the uncertainties in these quantities (within the model and the size of the ensemple) that are often better than the experimental ones. . The CED method overcomes the common equilibration problems with condensed phase molecular dynamics, i.e., how to choose initial molecular configurations not far from equilibrium at normal densities. Significant amounts of simulation time are usually required to equilibrate the badly packed molecules often generated with Monte Carlo methods. In particular to obtain densely packed polymers with their enormosous number of torsional degrees of freedom , often leads to highly nonequilbrium dihedral populations. Thus, care must be taken to generate an ensemble of thermally accessible conformations not far from equilibrium. These two requirements, condensed phase densities and equilibrated molecular conformations, are satisfied through the following method[15]

1. A cubic periodic unit cell containing a given number of molecules is built at 50% of the target density. Generally four polymer chains are sufficient although for very high molecular weights even one chain can be adequate. For the solvents, between 16 to 64 solvent molecules are adequate. We find that for building the structure it is useful to scale Van der Waals radii by a factor of 0.30 to get initial strucures that will eventually lead to a good ensemble.[16] For convenience in this paper, we used the experimental density of the solvents and polymers as a target value since they are available, however, systems with unknown density, would only require one additional step of NPT dynamics to obtain the trial density for CED.
2. The initial polymer amorphous structures are constructed using the rotational isomeric state (RIS) table and a suitable Monte Carlo procedure[16] to achieve a correct distribution of conformational states in the low density sample.
3. The charges of the isolated solvent or polymer molecules are defined using the charge equilibration method[13] or are obtained from quantum mechanical calculations.
4. The force field parameters are taken from a suitable force field, such as the generic Dreiding forcefield[6], Universal force field (UFF[35]) etc
5. Minimization: The potential energy of the bulk system is minimized for 5000 steps or until the atom rms force converges to 0.10 kcal/mol-Å.
6. Dynamics: 750 steps of Molecular Dynamics (1 femtosecond/step) at a temperature of 700 K using canonical fixed volume dynamics (NVT) are carried out to anneal the sample.
7. Compression: The reduced cell coordinates are shrunk such that the density is 64% of the target density.
8. The atomic coordinates are minimized and dynamics is done on the system with the previously described procedure holding the cell fixed (steps 5-6).
9. A total of five compression, minimization, and dynamics cycles are performed until the density reaches 120 % of the target density.
10. The cell parameters are increased in five cycles of expansion, minimization and dynamics, until the target density is reached.
11. Finally, the sample is allowed to relax in a minimization involving the cell and the atomic

coordinates.

12. Molecular dynamics are performed for 20 picoseconds. The first 10 picoseconds are used for thermalization of the sample at the desired temperature. The last 10 picoseconds are used for averaging of cell volume and potential energies (dispersion of van der Waals, polar or Coulomb, and hydrogen bonding).
13. The Hansen enthalpy components are calculated by subtracting the potential energy of the bulk system from the sum of the potential energies of the individual molecules as if separated by an infinite distance.
14. This process is repeated ten times with different initial random conformations and packing.
15. Hansen solubility parameters and molar volumes are computed as well as their standard deviations. 95% confidence limit, two standard deviations from the average value, are used to identify outliers. Typically none or at most two outliers are encountered in a ten sample run.

Hildebrand and Hansen solubilities are calculated from the molecular dynamics average energy components of the condensed phase simulation, single unit cell E_c, the energy components of the individual molecules, E_i, and the volume of the simulated sample, V_c as follows

$$\delta = \left(\frac{\Delta H_{vap} - RT}{V_m} \right)^{1/2} = \left(\frac{\sum_{i=1}^{n} < E_i - E_c > - RT}{N_o < V_c / n >} \right)^{1/2} \quad (3)$$

where < > indicates a time average over the duration of the dynamics, n the number of molecules and N_o is Avogadro's number. When E_i is taken to be the total energy, the value of δ is the Hildebrand solubility parameter, or one of the components, $E_{H\text{-}bond}$, $E_{coulomb}$, $E_{dispersion}$, which results in the Hansen solubility parameters. We stress the importance of using the thermally equilibrated ensemble of molecular conformations to estimate the gas phase term E_i, instead of n times the minimized energy of one molecule. For simplicity the gas phase ensemble average is approximated by the average of the isolated molecules taken from the condensed phase simulation, averaged over the entire molecular dynamics at the desired temperature.

The builder converts an existing model into an amorphous structure by manipulating the model's rotatable bonds. Each unique torsion can be defined using a Monte Carlo procedure with statistical weights given by a previously built rotational isomeric state table.[16] Conformations are rejected if two or more atoms come in contact closer than a van der Waals scale distance. The resulting amorphous structure can then be relaxed. In polymer calculations, the number of monomers in each chain is usually determined such that the total volume of the four chains is approximately 5900 Å^3. Alternatively, a degree of polymerization of 30 suffices to give converged values. In such polymer samples, the minimum number of atoms is around 1000. The overall procedure is illustrated in Figure 1.

2.0 Results

Over sixty common solvents, reactants, and monomers of significantly different structure, polarity, and chemical composition were chosen from various experimental compilations of Hildebrand solubility values available in the literature. Quantum Mechanical (Hartree Fock 6-31G** full geometry optimization, Mulliken and electrostatic potential (ESP) with a constraint to reproduce the quantum dipole moment from the wavefunction) charges were assigned to the molecules for ten separate independent molecular dynamics simulations. Table I (attached after references) contains the averaged results of 10 CED simulations for the two charge assignment methods for each solvent molecule. For comparison the various experimental values found in the literature and their deviations are included. Table II gives an example of the output of the CED procedure.

Figures 2 and 3 show the correlations between experimental and predicted values. Based on this data the accuracy of the CED method is 0.8 hildebrands. The experimental RMS value calculated from the various literature sources is 0.43 hildebrands. Although most solvents fall within the experimental error a few predictions are clearly outside the range of measured values. Exclusion of the six worst cases (formic-acid, acetic acid, dichlorodifluoromethane, acrylic acid, methyl formamide, and malononitrile) from the predictions reduces the RMS to 0.6 hildebrands.

The accuracy of the molecular dynamics results directly depends on the accuracy of the intra and inter-molecular potential atomic parameters (force field) and to some extent on the modeling protocol. This problem is in part overcome with force fields that accurately reproduce the experimentally measured bond distance, angles, as well as the respective force constants of small molecules. Less effort has gone into optimizing the van der Waals parameters in such force fields. Precision on the other hand is strongly dependent on the molecular dynamics procedure employed to prepare the samples. No significant differences in precision were found for the worst six cases (0.60, 0.62, 0.40, 0.37, 0.57, 0.42 hildebrands respectively) when compared to the average precision across all solvents (0.44 hildebrands).

We speculate that the assigned van der Waals force field parameters (our generic force field was not particularly fitted to halogens and nitrogen containing compounds) play a role in the accuracy of our predictions. We made no attempt to adjust the force field parameters here. However we point to the possibility of using the CED method together with experimental heats of vaporization and densities for the estimation of van der Waals Lennard-Jones parameters and/or the hydrogen bond terms for the various chemical atom types represented by these compounds. For example, systematic underestimation of the solubility parameter is observed through the calculated versus experimental ratio $\delta_{esp}/\delta_{exp}$ for alcohols and amides (2-ethyl-1hexanol 0.89, 2-ethyl-1-butanol 0.92, 1-pentanol 0.95, n-butanol 0.92, n-propanol 0.91, furfuryl alcohol 0.96, ethanol 0.87, 1,3-butanediol 0.91, methanol 0.89, N,N-dimethylacrylamide 0.91, dimethylacetamide 0.94, dimethylformamide 0.87, methylformamide 0.84). This suggests that the Dreiding parameters for the H-bond term (Do=2.5 Kcal/mol, Ro=3.2 A) could be modified to increase the accuracy of the predictions. Both parameters may be involved since the density of these two groups of compounds is also underestimated. Finally, there seems to be a systematic overestimation of the solubility parameter for the organic acids. The $\delta_{esp}/\delta_{exp}$ ratio is consistently high (propionic acid 1.18, acetic acid 1.30, methacrylic acid 1.04, formic acid 1.30, acrylic acid 1.21). The effect is

opposite the hydrogen bond effect previously mentioned. We assume that the molecules in the gas phase are non-interacting. Many low molecular weight acids exist in a dimerized form in the gas phase. If we assume that half of the intermolecular hydrogen bonds are preserved in the gas phase, the solubility parameter will be decreased by about 3 hildebrands, bringing theory and experiment quite close in agreement. We now discuss the effect of charge assignment methods.

Although Mulliken charges are quite useful in determining the structure of molecules in the gas phase these appear to be less accurate than Electrostatic Potential charges (ESP) for the determination of condensed phase properties. We advocate the use of ESP charges for the estimation of solubility parameters and the use of Mulliken charges for conformational studies in the gas phase. It appears that the far field representation of the ESP charges captures more accurately the physical interactions between molecules in the condensed phase.
We compare our Molecular Dynamics results to other predictive methods available in commercial software packages such as Synthia-Fedors and Synthia-van-Krevelen.[25] These methods can be considered state-of-the-art group additivity methods, relying on topological descriptors and other single molecule quantities to make predictions based on correlations and parameter extractions from large databases of solubility parameters. Although intended for predictions on polymers these parametric methods require only the isolated monomer structure to make a prediction. The methods are fast and simple to use. In contrast, the MD method presented here requires a full condensed phase simulation of the compound of interest. Nonetheless the CED Molecular Dynamics method is non-parametric. Beyond the predetermined force field, in our case a generic force field published in the mid 80's, CED used no adjustable parameters and no experimental input information. Moreover, in principle the CED molecular dynamics method can make predictions as a function of pressure and temperature and it is general enough to deal with complex mixtures, including solvent/polymer mixtures. The average root mean square (RMS) difference for the CED results and for two group additivity predictive methods, Synthia-Fedors and Synthia-van-Krevelen[5] with respect to the experimental values is shown Table III

Solubility parameters predicted employing the current molecular dynamics simulation methodology can also be compared to those calculated employing molecular dynamics simulations by Rigby et al.[26a]. Employing the PCFF forcefield and Amorphous Cell/Discover programs,[25] Rigby et al. predict solubility parameters for 13 of the molecules in Table I which have an average absolute difference with experiment of 0.92 $(cal/cm^3)^{1/2}$ which is similar to that predicted by the current methodology (absolute difference of 1.1 for the 13 molecule set). As with the current simulations, the largest differences in the set are seen for two acid molecules. The current authors have calculated the solubility parameters for hexane, acetone, and n-propanol employing molecular dynamics simulations with the COMPASS forcefield and Amorphous Cell/Discover programs[25]. Average absolute differences with experiment for this set of three was found to be 0.25 with COMPASS methodology which is slightly smaller than the 0.55 difference observed for the current CED methodology. The COMPASS forcefield has been extensively optimized to reproduce the heats of vaporization of a large number of organic liquids. For example, in a related COMPASS forcefield study,[26c] Sun has calculated heats of vaporization for 100 compounds to within an average percent error of experiment of -0.2% with maximum errors of 14.6% and 14.5%. This is to be contrast with our current approach where generic force field was employed without any further optimization. Eichinger and coworkers[26b] have employed the COMPASS forcefield to compute solubility parameters for Ultem oligomers, related molecules, and solvent molecules including toluene. Not surprisingly the calculated solubility parameter for

toluene is 0.07 $(cal/cm^3)^{1/2}$ closer to the average experimental value (8.94 $(cal/cm^3)^{1/2}$) than the previous PCFF forcefield value.[26a] The calculated toluene solubility parameter value of 9.0 $(cal/cm^3)^{1/2}$ compares well to the current ESP calculated solubilty parameter of 9.23 $(cal/cm^3)^{1/2}$.

2.1 Application to the Electronic Nose

An electronic nose has been built at Caltech[27-29] employing an array of polymer sensors. Sensors are built with conducting leads connected through thin film polymers loaded with carbon black. Odorant detection relies on a change in electric resistivity, ΔR/R, of the polymer film as function of the amount of swelling caused by the odorant compound. The amount of swelling depends upon the chemical composition of the polymer and the odorant molecule. An array of twenty carbon black loaded polymers give rise to a specific change in resistivity patterns upon exposure to a given molecular species. The pattern is unique and unambiguously identifies the compound.[28,29]

The experimentally determined changes in relative resistivity, ΔR/R, of seven polymer sensors upon exposure to twenty-four solvent vapors was correlated with the calculated Hansen solubility components. The permeability of a given odorant in a polymer is given by[20]

$$P = A\exp\left(\frac{\Delta H_s}{k_B T} - \frac{E_D}{k_B T}\right) \qquad (4)$$

where A is the pre-exponential factor related to entropy, ΔH_s is the heat of sorption of the solute and E_D is the activation energy for diffusion of the molecule in the polymer. We assume that the relative change in resistivity is directly proportional to the odorant's permeability. The following expression was used to correlate ΔR/R with the Hansen components of the cohesive energy of the polymer and solvent as well as the molar volume of the solvent.

$$\Delta R / R = R_o \exp(-\gamma V_s)\exp[\sum_{i=1}^{3} \beta_i(\delta_i^s - \delta_i^p)] \quad (5)$$

γV_s is the activation energy of diffusion of the solute in the polymer, proportional to the molar volume of the odorant, V_s. The exponential factor γ is a best-fit parameter. We base this relation on the experimental observation that the diffusion coefficients of various molecules is linearly related to the molar volume of the solute in the case where the actual temperature is greater than the glass transition (T_g) of the polymer.[31] This approximation is used in our analysis regardless of T_g. δ_i^s (i=1,2,3) are the cohesive energy density component of the solvent s, where i=1, 2 and 3 refer to the electrostatic, dispersion and hydrogen bond components respectively. Similarly, δ_i^p is the i-th cohesive energy component of the polymer sensor p. The exponential coefficients β_i are treated as best fit parameters as well as is the pre-exponential term R_0. It should be noted that we preserve the sign of the energy components in equation (5), usually lost in the definition of Hansen and Hildebrand parameters. This is important because such interactions can be attractive or repulsive, depending on the polymer/odorant mixture in question. For simplicity we employed the charge equilibration, Qeq,[13] method to assign atomic charges to polymers and solvent molecules.

The results of fitting equation (5) to experimental changes in resistivity[34] are shown in Figure 4 for seven electronic nose polymer sensors and twenty-four solvents.[27] Pearson's correlations between the experimentally determined change in resistivity and the Hansen solubilities are shown for polymer sensors (poly(methylmethacrylate) (PMMA), poly(4-hydroxystyrene) (P4HS), polyethyleneoxide (PEO), polyethylene (PE), poly(ethylenevinyl acetate) (PEVA), polysulfone, and caprolactone) in Table IV. The calculated Hansen solubilities for the seven polymers and twenty-four solvents are summarized in Table V.

The correlation was particularly good for polysulfone, poly(4-hydroxystyrene) and PEVA (polyethylene-co-vinyl acetate) and especially poor for polymethylmethacrylate based on both correlation slope and the Pearson R values for the linear fit. Polysulfone appears to discriminate between solvents of different sizes since the free volume fraction is small and the free volume distribution may be narrow, resulting in a "molecular sieve" effect. Additionally, the experimental relative change in resistivity in polysulfone ranges from zero to 1.0, which makes it a particularly good high-resolution sensor.

The polyethylene-co-vinyl acetate detector also correlates reasonably well with the theoretical relative change in resistivity. However, the relative change in resistivity range is smaller compared to polysulfone indicating that it is less discriminating towards ester and alcohol solvents. A possible explanation that accounts for this observation is that PEVA contains polar ester functional groups due to the vinyl content (18 %), as well as non-polar components due to the polyethylene content (82 %). PEVA has a glass transition below room temperature and as a result contains a large free volume fraction. This decreases the sensitivity towards molecules of different sizes compared to high T_g polymers such as polysulfone. The third particularly good detector in terms of signal correlation with theoretical prediction is poly(4-hydroxy styrene). This detector is particularly sensitive to molecules functionalized with highly polar groups such as alcohol due to the hydroxyl functional group. However, the sensitivity of this sensor to moderately polar or non-polar solvents such as esters is particularly low.

3.0 Conclusions

The CED Molecular Dynamics method presented here provides a reproducible method to predict the Hildebrand solubility parameters for polymers and solvents. Its precision (0.44 hildebrands) is comparable to the experimental error (0.43). We investigated the use of compression and expansion cycles, simulated annealing, charge assignment methods, and statistical sample averaging. It is important to start from a low-density sample to achieve equilibrated conformational statistics within a reasonable computational time. Ten samples, with roughly 1,000 atoms each, seem adequate to estimate these properties.

The results compare well with experimental values, although accuracy (0.88 hildebrands) is somewhat lower than precision (0.44 hildebrands), mostly a deficiency of the force field. No attempt was made to refine the force field parameters to improve the accuracy of the method, although such a possibility is clearly present. The present method should be added to the existing methods (ab initio EOS, x-ray structure fittings) currently used to estimate Lennard-Jones parameters or hydrogen bond parameters.

The CED Molecular Dynamics calculated Hildebrand and Hansen parameters give systematic measures of the solvency of a given chemical compound. Such values are of practical use for the design of new materials, formulations, and processes. As parallel molecular dynamics algorithms are implemented simulation times will be reduced and the prediction of solubility parameters will become even more practical. For example, the estimation of Hildebrand and Hansen solubility parameters takes approximately two hours in a dual processor Linux computer. Using a highly parallel particle-mesh algorithm[32-33] to integrate the dynamics, the CPU times can be reduced to ten minutes using twenty four processors. In such a computational environment, it becomes practical to automate the population of databases of solvents and complex mixtures with Hildebrand and Hansen solubility parameters for product formulation work.

3.1 Acknowledgements

This work was supported by an ARO/MURI and in part by a grant by the 3M Company and Owens Corning. The facilities of the MSC were partly funded by NSF MRI and ARO/DURIP and are also supported by grants from DOE-ASCI, Chevron, NIH, ONR, Seiko-Epson, Avery-Dennison, Kellogg's, General Motors, Beckman Institute, Asahi Chemical, and Nippon Steel.

References

1. J.H. Hildebrand, The Solubility of Non-Electrolytes. New York: Reinhold, (1936).
2. Hansen, C.M., J Paint Technol **39**, 511, (1967).
3. P. Choi, T.A. Kavassalis, and A. Rudin, J. Coll. Interface Sci., **150**, 386 (1992).
4. T.A. Kavassalis, P. Choi, and A. Rudin, Molecular Simulation **11**, 229 (1993).
5. E. Rogel, Energy & Fuels **11**, 920 (1997).
6. M. Kotelyanskii, Trends Polym. Sci. **5**, 192 (1997).
7. R. Khare, M. E. Paulaitis, S. R. Lustig, Macromolecules **26**, 7203 (1993).
8. R. F. Rapold, U. W. Suter, D. N. Theodorou, Macromol. Theory Simul. **3**, 19-4 (1994).
9. R. J. Roe, D. Rigby, J. Phys. Chem. **89**, 5280 (1988).
10. H. Furuya, M. Mondello, H. J. Yang, R. J. Roe, Macromolecules **27**, 5674 (1994).
11. R. J. Roe, Computer Simulation of Polymers. R. J. Roe, Ed., Polymer Science and Engineering, Prentice-Hall, New Jersey (1991).
12. A. A. Gusev, M. M. Zender, U. W. Suter, Macromolecules **27**, 615 (1994).
13. A. K. Rappe.; W. A. Goddard, III; Journal of Physical Chemistry **95**, 3358 (1991).
14. (a) D.W. van Krevelen; Properties of Polymers: Their Correlation with Chemical Structure; their Numerical Estimation and Prediction from Group Contributions, Elsevier Science Publishers, NY, pg 536. (b) Ibid p. 575 (1990).
15. Belmares, M.P., "Molecular origins of the thermophysical properties of polymers and modeling of polymer permeation by large molecules", Caltech Thesis (Ph. D.), UM #9916173, 1998. The procedure has been coded as a single application using the Software Developer's Kit (SDK) in Cerius2, Version 4.0, Accelrys, Inc. San Diego, CA.
16. Originally part of the suite of programs in Polygraf, the amorphous builder is part of the Cerius2 software package, Cerius2, Accelrys, Inc. San Diego, CA.
17. S.L. Mayo, B.D. Olafson, W.A. Goddard III J. Phys. Chem. **94**, 8897 (1990).
18. K.L. Hoy, J. Paint Technology **42**, 79 (1970).
19. "Polymer Handbook", ed J. Brandrup, E.H. Immergut, and E. A. Grulke, 4th ed., J. Wiley, New York (1999).
20. 60th edition, CRC Handbook of Chemistry and Physics, ed., Robert C. Weast and Melvin J. Astle, CRC Press, Boca Raton, Fl, pgs. 732-735 (1980).
21. Principles of Polymer Systems, ed., Ferdinand Rodriguez, 2nd Ed, McGraw-Hill, New York, pg 25-26 (1982).
22. Physical Properties of Polymers - Prediction and Control, A. Askadskii, Gordon and Breach, Amsterdam, pg. 41-48 (1996).
23. 2nd edition, CRC Handbook of Solubility Parameters and Other Cohesion Parameters, A. F. M. Barton Ed. Boca Raton, Fl, pgs. 94-110, 153-159, CRC Press (1991).
24. "Graphic Analysis of Resin Solubilities", ed. Jean P. Teas **40**, No. 516 (1968).
25. Computational results obtained using software programs from Accelrys, Inc. San Diego, CA. Property/structure solubility parameters calculated employing Synthia program. Molecular dynamics results obtained employing the COMPASS forcefield with Amorphous Cell/Discover Programs.
26. a. B. E. Eichinger, D. R. Rigby, and M. H. Muir, Comp. Pol. Sci. **5(4)**, 147 (1995); b. B. E. Eichinger, D. R. Rigby, and J. Stein, Polymer **43,** 5999 (2002); c. H. Sun, J. Phys. Chem. B. **102**, 7338 (1998).
27. G. Walker, N. Lewis, private communication.

28. E.J. Severin, B.J. Doleman, and N.S. Lewis, Analytical Chemistry **72**, 658 (2000).
29. M.C. Lonergan, E.J. Severin, B.J. Doleman, S.A. Beaber SA, R.H. Grubb, N.S. Lewis, Chemistry of Materials **8**, 2298 (1996).
30. Newman, S., *Polymer Blends,* D. R. Paul, Ed., Academic Press, Inc., Orlando, vol. 1, (1978).
31. D. W. V. Krevelen, *Properties of Polymers*: Their Correlation with Chemical Structure; their Numerical Estimation and Prediction from Group Contributions, Elsevier Science Publishers, New York, (1990).
32. S. J. Plimpton, R. Pollock, M. Stevens, Proc of the Eighth SIAM Conference on Parallel Processing for Scientific Computing, Minneapolis, MN, March (1997).
33. S. J. Plimpton, "Fast Parallel Algorithms for Short-Range Molecular Dynamics", J Comp Phys **117**, 1 (1995).
34. Severin, E.J.; "*Array-based vapor sensing using conductive carbon black-polymer composite thin film detectors",* Caltech Dissertation, 1999, ISBN 0-599-42672-
35. A. K. Rappé, C. J. Casewit, K. S. Colwell, W. A. Goddard III, and W. M. Skiff; J. Am. Chem. Soc. 114, 10024 (1992)

Table I. Comparison of calculated and experimental solubility parameters for 65 common solvents, reactants, and monomers in order of increasing experimental Hildebrand solubility parameter.

Compound	Exptl. δ [a]	Std. Dev.	Mulliken δ [b]	Std. Dev.	ESP	δ[c]	Std. Dev.	Ref.[18]	Ref.[19]	Ref.[20]	Ref.[21]	Ref.[22]	Ref.[23]	Ref[24]
dichlorodifluoromethane	5.81	0.44	10.89	0.36	8.52	0.4		5.5				6.13		
neopentane	6.30	-	7.3	0.88	7.18	0.68		6.3						
1,3-butadiene	7.10	0.39	7.32	0.38	7.33	0.68	7.77	7.1	7.1					
hexane	7.24	0.02	7.47	0.47	7.38	0.69	7.27	7.3	7.3	7.3	7.3	7.30	7.24	
heptane	7.40	-	7.55	0.34	7.46	0.58		7.4						
diethyl ether	7.62	0.16	8.92	0.4	7.45	0.57	-	7.4	-	7.4	7.4	7.74	7.62	
di-propyl amine	7.79	0.10	7.42	0.5	8.42	0.2	7.97		-	-	-	7.79	7.79	
di-ethyl amine	7.96	0.03	7.61	0.33	8.66	0.58	8.04	8	-	-	-	7.99	7.96	
di-Isobutyl-ketone	8.17	0.25	8.68	0.44	8.55	0.27	-	7.8	-	-	-	8.28	8.17	
cyclohexane	8.18	0.42	8.44	0.33	8.59	0.37	8.19	8.2	9.3	8.2	8.2	8.23	8.18	
n-butyl methacrylate	8.20	0.00	9.61	0.44	9.01	0.38	-	8.2	-	-	8.2	-	-	
ethyl methacrylate	8.35	0.07	10.76	0.62	9.75	0.24	-	8.3	-	-	8.4	-	-	
1-chlorobutane	8.44	-	8.19	0.2	8.78	0.32		-	-	-	-		8.44	
methyl-isobutyl-ketone	8.57	0.12	9.68	0.3	9.12	0.38	-	8.4	-	-	-	8.33	8.57	
ethyl acrylate	8.60	0.21	11.22	0.71	10.4	0.32	8.81	8.6	-	-	8.4	-	-	
2-ethylhexyl acrylate	8.64	0.05	8.58	0.32	8.99	0.44	7.87	7.8	-	-		-	-	
carbon tetrachloride	8.65	0.05	9.64	0.45	9.32	0.29	8.55	8.6	8.6	8.6	8.6	8.72	8.65	
n-butyl acrylate	8.68	0.20	10.18	0.47	9.38	0.46	8.63	8.5	-	-	8.9	-	-	
ethyl benzene	8.80	0.04	9.48	0.26	9.33	0.41	8.84	8.8	-	8.8	8.8	8.72	8.80	
ethyl chloride	8.85	0.49	8.21	0.54	8.23	0.7	-	9.2	-	-	8.5			
methyl methacrylate	8.91	0.28	11.62	0.55	9.69	0.4	9.23	8.8	-	-	8.7		-	
toluene	8.94	0.08	9.56	0.2	9.23	0.66	8.95	8.9	8.9	8.9	8.9	9.11	8.91	

1,4 dioxane	9.02	1.58	13.2	0.24	10.3	0.5	10.13	7.9					
tetrahydrofuran	9.10	-	11.44	0.37	9.64	0.49		9.1					
benzene	9.15	0.03	10.34	0.47	9.84	0.51	9.16	9.2	9.2	9.2	9.15	9.11	9.15
methyl-ethyl-ketone	9.27	0.06	9.88	0.27	9.43	0.37	9.45	9.3	-	9.3	9.3	9.31	9.27
styrene	9.30	0.25	9.85	0.4	9.74	0.36	9.35	9.3	9.3	9.3	8.66	9.31	9.30
diethyl phthalate	9.55	0.05	11.3	0.38	10.2	0.47	9.97	10	-	-	10.05	10.09	-
chlorobenzene	9.57	0.07	10.32	0.39	10.5	0.5	9.67	9.5	-	9.5	9.5	9.60	9.57
tetrahydronaphthalene	9.60	0.17	9.89	0.41	9.75	0.31	9.5	9.5	-	-	-	9.80	-
acetone	9.77	0.15	10.79	0.5	10.2	0.59	9.62	9.9	-	10	10	9.80	9.77
2-ethyl-1-hexanol	9.85	0.33	8.97	0.54	8.75	0.45	10.15		9.5	-	-		9.85
cyclohexanol	9.88	0.27	10.15	0.47	10.5	0.47	10.42	9.9	9.9	9.9	-	9.60	9.88
o-dichlorobenzene	9.98	0.03	10.56	0.2	10.3	0.25	10.04	10	-	-	-	10.05	9.98
propionic acid	10.16	2.20	11.73	0.25	12	0.49	12.47	9.9	8.1				
cyclohexanone	10.16	0.37	10.35	0.44	9.87	0.38	10.42	9.9					
acetic acid	10.35	1.31	12.88	0.66	13.5	0.62	13.01	10.2	10.1	-	12.6	10.49	10.35
2-ethyl-1-butanol	10.38	0.74	9.15	0.46	9.52	0.35	-	10.5	11.9	-	-	10.39	10.38
1-pentanol	10.60	0.47	9.51	0.18	10.1	0.48	11.12	-	11.6	-	-	10.63	10.60
propionitrile	10.73	0.07	11.03	0.33	10.2	0.46	10.73	10.8	-	10.8	10.7	10.63	-
N,N-dimethylacrylamide	10.80	-	11.07	0.36	9.86	0.37	-	10.8	-	-	-	-	-
dimethylacetamide	10.80	-	11.13	0.39	10.1	0.42		10.8					
methacrylic acid	11.20	1.10	10.94	0.48	11.6	0.45	13.11	11.2	11.2				
n-butanol	11.30	0.84	9.89	0.56	10.4	0.46	11.6	11.4	13.6	11.4	11.4	11.32	11.30
N-methylpyrrolidinone	11.30	-	11.54	0.41	10.6	0.35	-	11.3	-	-	-	-	-
acetonitrile	11.92	0.11	11.58	0.55	12.5	0.49	12.11	11.9	11.9	11.9	11.9	11.96	11.75
dimethylformamide	11.95	0.22	11.97	0.47	10.4	0.14	11.79	12.1					
n-propanol	11.97	0.57	10.28	0.43	10.9	0.6	12.18	11.9	10.5	11.9	11.9	12.01	11.97

formic-acid	12.15	1.28	15.6	0.51	15.8	0.59		12.1	14.7			12.20	12.15
acrylic acid	12.30	0.51	14.49	0.28	15	0.37	12.89	12	12	-	-	-	-
furfuryl alcohol	12.50	-	13.79	0.3	12	0.27		12.5					
γ-butyrolactone	12.74	0.19	14.57	0.33	12.6	0.31	12.87	12.6					
y-butyrolactone	12.79	0.13	13.99	0.26	12.7	0.3	12.87	12.6	-	-	-	12.89	12.78
ethanol	12.92	0.12	11.75	0.64	11.2	0.51	12.78	12.7	-	12.8	12.7	12.99	12.92
propiolactone	13.30	-	15.05	0.33	13	0.46		13.3					
propylene carbonate	13.33	0.04	14.64	0.41	13.1	0.48	-	13.3	-	-	-	13.38	13.3
maleic anhydride	13.60	-	17.18	0.5	14.8	0.28		13.6					
1,3-butanediol	14.14	1.59	12.67	0.33	12.8	0.52	13.76	11.6	10.9	-	-		14.14
methanol	14.30	0.08	12.91	0.55	12.6	0.71	14.5	14.5	14.5		14.5	14.50	14.3
dimethyl sulfoxide	14.50	-	14.71	0.34	15.6	0.57		14.5					
ethylene carbonate	14.60	0.11	16.88	0.33	14.7	0.39	-	14.7	-	14.7	14.5	14.50	-
malononitrile	15.10	-	14.74	0.31	12.9	0.42		15.1					
succinic anhydride	15.40	-	16.76	0.46	15.2	0.4		15.4					
glycerol	15.50	3.63	16.51	0.82	15.6	0.32	17.69	16.5	9.9	16.5	16.5		21.1
methyl formamide	15.75	0.49	14.11	0.38	13.3	0.57		16.1	15.4				
Average std dev		**0.43**		**0.42**		**0.44**							

[a] Average of experimental values, references 18-24, in (cal/cm^3) -
[b] Simulations employing Mulliken charges
[c] Simulations employing electrostatic potential charges

Table II. Example of output from the CED molecular dynamics method. Here the simulation procedure used ten samples to estimate the condensed phase properties of 2-ethylhexylacrylate.

Sample	Cohesive Energy (cal/cc)	Solubility Parameter (cal/cc)$^{1/2}$	Density (g/cc)	End-End distance (A)	Radius Gyration (A)	Hansen Solubilities Elec	Dispersion H-Bond (cal/cc)$^{1/2}$
1	-73.42	8.57	0.80	7.10	3.19	3.52	7.56	0.00
2	-81.04	9.00	0.88	6.78	3.19	4.05	8.31	0.00
3	-67.84	8.24	0.83	7.17	3.17	3.20	7.72	0.00
4	-77.06	8.78	0.83	7.63	3.26	3.60	7.84	0.00
5	-70.63	8.40	0.84	7.33	3.17	3.60	7.86	0.00
6	-70.46	8.39	0.82	6.67	3.22	3.18	7.72	0.00
7	-77.91	8.83	0.87	7.34	3.13	3.42	8.21	0.00
8	-81.90	9.05	0.87	7.17	3.19	4.00	8.15	0.00
9	-70.78	8.41	0.85	6.82	3.18	3.81	7.94	0.00
10	-65.89	8.12	0.82	6.74	3.19	3.96	7.87	0.00

	Average	Standard Deviation
Density	0.84 +-	0.03 (g/cc)
Cohesive Energy Density	-73.69 +-	5.52 (cal/cc)
Solubility Parameter	8.58 +-	0.32 (cal/cc)$^{1/2}$
	17.55 +-	0.66 (Mpa)$^{1/2}$
Electrostatic Hansen SP	3.63 +-	0.32 (cal/cc)$^{1/2}$
Dispersion Hansen SP	7.92 +-	0.24 (cal/cc)$^{1/2}$

Table II (Example Output of CED Simulation) Continued:

Hydrogen Bond Hansen SP	0.00 +-	0.00 (cal/cc)$^{1/2}$
Non-Bond EEX	-76.05 +-	5.49 (cal/cc)
Unit Cell Volume	5820.43 +-	174.32 A^3
End-to-End Distance	7.07 +-	0.3134 (A)

Radius of Gyration 3.19 +- 0.0334 (A)

Table III. Average error of Synthia predictive methods compared with CED predictions of Hildebrand Solubilities.

Method	RMS [a]
CED-ESP	0.806
Synthia-Fedor	1.388
Synthia-van-Krevelen	1.202

[a] Root mean square deviation (hildebrands).

Table IV. Pearson's correlation coefficients and slopes of predicted versus experimental changes in resistivity, $\Delta R/R$, for each of seven polymer vapor solvent detectors.

Polymer Sensor	Slope	Pearson's R
Polycaprolactone	0.858	0.925
Polysulfone	0.932	0.962
PMMA	0.678	0.827
PEVA	0.888	0.936
Polyethylene	0.870	0.933
Polyethyleneoxide	0.746	0.874
Poly(4-hydroxystyrene)	1.018	0.991

Table V. Estimated molar heats of vaporization and Hansen solubilities

	ΔH_{vap}	δ_1	δ_2	δ_3
Odorants	**Kcal/mol**	**Electrostatic**	**Dispersion**	**H-bonding**
2-pentanol	-151.42	-53.32	-76.48	-21.62
3-pentanol	-142.40	-47.89	-76.87	-17.64
amylacetate	-127.31	-40.19	-87.13	0.00
butylacetate	-132.03	-41.75	-90.28	0.00
decylacetate	-104.70	-21.02	-83.68	0.00
ethanol	-257.64	-146.00	-51.35	-60.29
ethylacetate	-159.31	-68.99	-90.33	0.00
hexylacetate	-122.55	-34.83	-87.72	0.00
iso-amylalcohol	-159.46	-59.82	-73.87	-25.77
isoamylacetate	-125.90	-38.67	-87.24	0.00
isoamylbenzoate	-119.56	-23.04	-96.52	0.00
isoamylbutyrate	-111.52	-25.34	-86.17	0.00
isoamylcaproate	-104.57	-20.83	-83.74	0.00
isoamylpropionate	-113.17	-30.36	-82.81	0.00
isobutylacetate	-130.92	-45.05	-85.87	0.00
isopropylacetate	-143.46	-57.20	-86.26	0.00
n-amylalcohol	-159.42	-59.53	-75.46	-24.44
n-heptanol	-130.23	-37.63	-76.59	-16.01
n-hexanol	-141.38	-46.42	-77.97	-16.99
n-propanol	-193.82	-94.68	-60.77	-38.37
octanol	-127.59	-33.80	-79.91	-13.88
octylacetate	-112.37	-26.42	-85.95	0.00
propylacetate	-142.96	-54.90	-88.06	0.00
n-butanol	-152.72	-64.31	-61.58	-26.82
Polymer Sensor				
PMMA	-90.51	-31.19	-59.32	0.00
P4HS	-106.66	-28.66	-64.48	-13.51
PEO	-168.10	-68.36	-95.90	-3.84
PE	-85.45	-1.00	-84.46	0.00
PEVA	-85.02	-10.82	-74.20	0.00
Polysulfone	-138.74	-29.76	-108.98	0.00
Caprolactone	-122.66	-35.31	-87.34	0.00

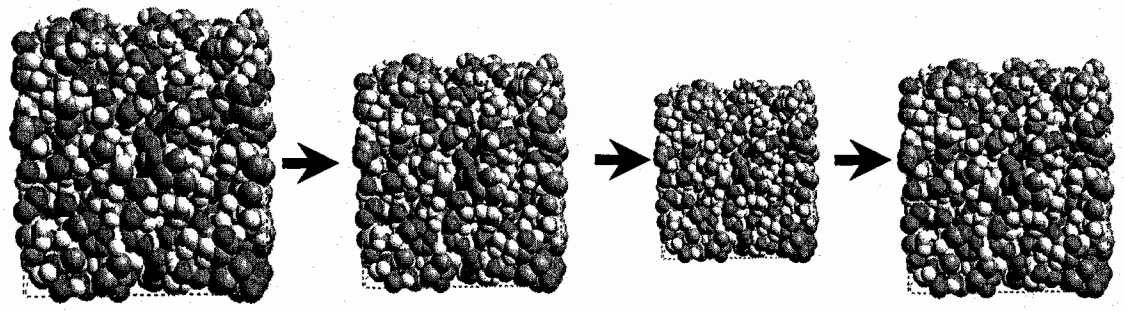

Figure 1. A polymer or solvent sample is put through a series of compression and expansion steps until the proper density and packing is obtained. On the left the initial density is 0.4 ρ_o, 40% of the target density. After compression, second step, the sample is over compressed to 1.2 ρ_o . Finally the sample is allowed to relax. Through NPT molecular dynamics a final prediction of the density and cohesive energy of the sample is obtained. The process is repeated for a few samples to gather statistics.

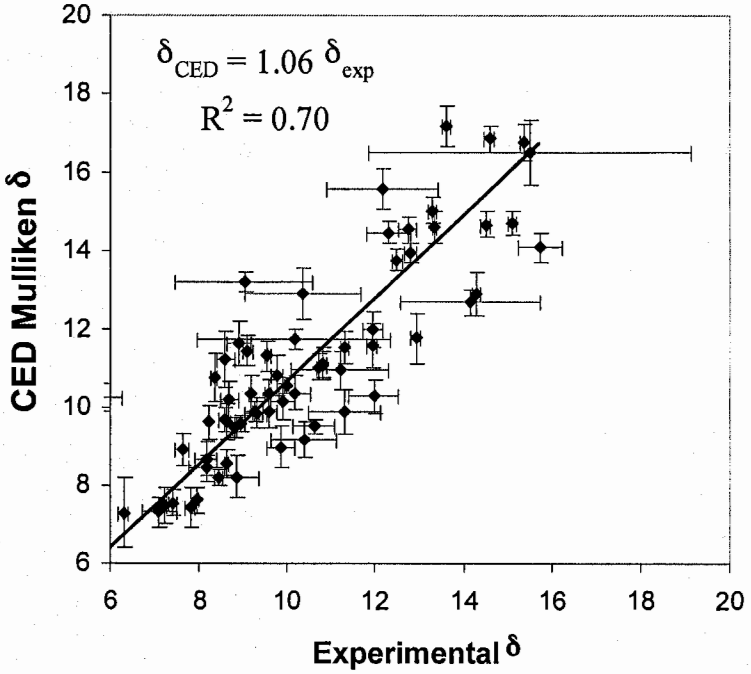

Figure 2. CED versus experimental Hildebrand solubility parameters for all molecules in Table I. Error bars indicate one experimental and simulation standard deviation. Charge assignment method is HF 6-31G** Mulliken population charges.

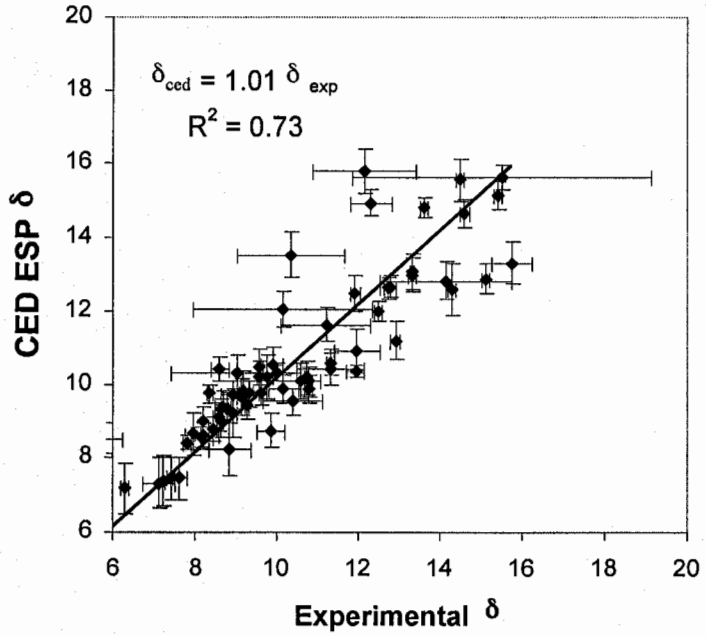

Figure 3. CED versus experimental Hildebrand solubility parameters with quantum mechanical electrostatic potential (ESP) HF 6-31G** assigned charges. Error bars indicate one experimental and simulation standard deviation.

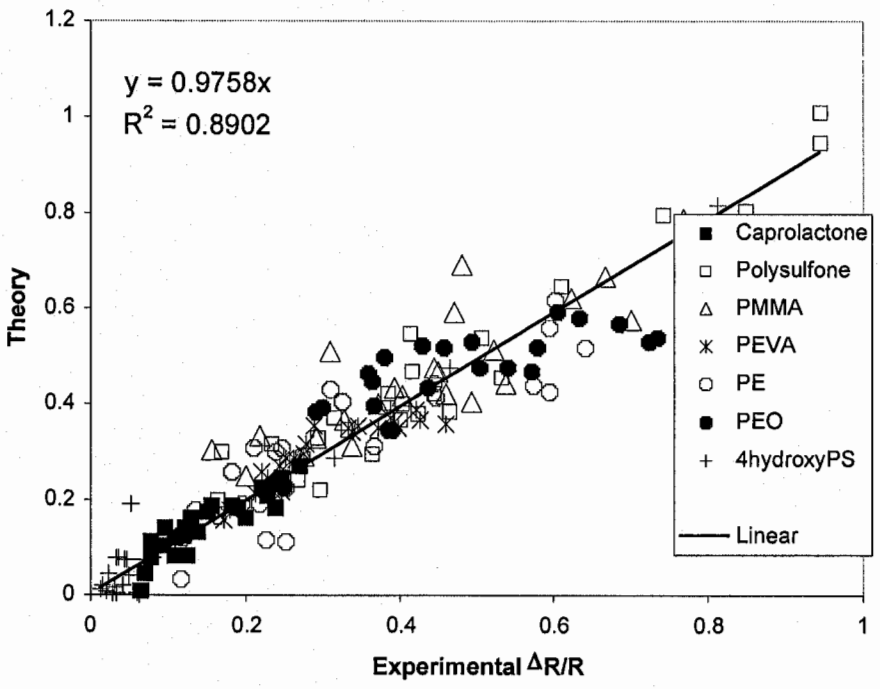

Figure 4. Comparison between theory, equation (5), and experimental changes in resistivity of seven polymer sensors exposed to twenty-four solvents.

Dr. Gordon Shepherd

Our subproject carried out several studies during the five years of the grant plus the final one year no-cost extension (overall 1998-2004). The overall aim of these studies was to provide computational analysis of key aspects of experimental data generated by our laboratory and by our collaborators that would give insight into the molecular and cellular basis of information processing of olfactory sensory input in the olfactory pathway.

Study 1. Interactions between odor molecules and receptor binding pocket. A major goal of our subproject was to gain insight into the nature of the information that is carried by the odor molecules and transferred into the neural domain by interactions with olfactory receptor proteins. The first study was carried out by Michael Singer, a graduate student in our laboratory. For his thesis work, supported in part by the MURI, tested by molecular modeling the ligand specificity of a specific receptor, I7, that had been shown in expression experiments to interact preferably with octanal, a straight-chain 8 carbon aldehyde. Using commercial software, he constructed model of I7 and carried out docking experiments, which showed that the model also preferred octanal over neighboring aldehydes. This analysis pointed to specific interactions between the OH group of the aldehyde and the positive nitrogen group on a specific lysine residue in a binding pocket, as well as weak interactions with other residues forming the walls of the pocket. This was among the first evidence for the specificity of the binding pocket in an expressed olfactory receptor. It was reported in Chemical Senses in 2000 (Singer, 2000).

In a parallel study we collaborated with the Goddard group in the MURI program to carry out a much more extensive study of receptor binding properties in a set of receptors that had been characterized physiologically by the Buck laboratory and shown to be correlated with specific receptors as identified by single cell PCR. This project is described in more detail in the Goddard progress report. This three way collaboration resulted in a paper (Floriano et al, 2000) which also showed that the model gave rank ordering of ligand preference similar to that seen in the experiments. Together, these studies supported by MURI have provided some of the first and most convincing evidence for a binding pocket in the 7TM olfactory receptors, and for the differential interactions between determinants of the odor molecules and specific residues within the binding pocket. They thus give direct insight into the elementary sensory units that are the basis for subsequent processing by circuits in the olfactory pathway.

In subsequent work Dr. Chiquito Crasto, with the assistance of Peter Bail, has continued Singer's work in collaborating with the Goddard and Buck laboratories to extend their computational study to further olfactory receptors and their interactions with odor ligands. Under the supervision of Drs. Shepherd, Miller and Nadkarni, he is also responsible for the olfactory receptor database (ORDB) and the odor ligand database (ODORDB), funded by a Human Brain Project grant, which support the analysis of odor ligand-olfactory receptor interactions, from which our collaborative study has benefitted.

It is widely assumed that genes map directly into behavior, and therefore that the lower numbers of olfactory genes in humans compared with rodents reflect a diminished importance of smell in humans. We have argued that this direct mapping cannot be assumed, and that other factors must be taken into account, which suggest that human smell is more important than generally realized (Shepherd, 2004).

Study 2. Gene chip analysis of expressed olfactory receptors. Although genomic DNA indicated the numbers of olfactory receptor genes in human and mouse (350 and 1200 respectively) it left unknown how many of these are actually expressed in the olfactory

epithelium. To answer this we have undertaken a collaborative study with the laboratory of Stuart Firestein in Columbia and Minghong Ma in my laboratory, who now is at U Penn, building the first Affymetrix gene chip for this purpose. Thus far the chips have been able to identify over 800 expressed genes (Zhang et al, in preparation). Further studies will use the chips for analysing expression in different organs and at different stages of development. A new database for receiving this chip data is in development, under the supervision of Drs. Shepherd, Miller and Nadkarni.

Study 3. Differential odor responses in populations of olfactory receptor cells. Most of our knowledge of the differential responses of olfactory receptor cells to different odors has been obtained from recordings from single cells. Because of the enormous number of different receptors, a high throughput recording method is needed. To answer this need we developed an isolated preparation of a segment ("swatch") of the epithelium, in which we could use Ca sensitive dyes to image the odor responses of up to several hundred cells at one time. This enabled us to characterize for the first time the simultaneous responses of many cells to the same odor, and to a battery of different odors (Ma and Shepherd, 2000). This same approach has been used to analyse for the first time the response selectivity of cells in the septal organ of the rat (Ma et al, 2003). To extend these studies we have collaborated with the laboratory of Peter Mombaerts to use gene targeted mice with cells expressing the MOR23 olfactory receptor gene tagged with GFP. A report is in preparation (Grosmaitre et al, 2003).

Study 4. Differential odor responses in populations of olfactory glomeruli. The differential odor responses of receptor cells are projected onto the glomeruli of the olfactory bulb, giving rise to spatial patterns of activity reflecting the differential responses of the individual glomeruli (also called odor maps or odor images). Building on our study of aldehyde responses of the I7 receptor (see above) we have carried out a study of the odor images elicited by the different aldehydes. For this we have used high resolution fMRI, which we introduced several years ago for olfactory studies in collaboration with the imaging group at Yale under Robert Shulman and Douglas Rothman. For this study we drew on our Human Brain Project expertise to develope methods for rendering the 3D image as flat maps (Liu et al, 2004). The results (Xu et al, 2003) show that the images are overlapping but different for the different carbon chain lengths of the aldehydes. These fMRI maps have the advantage of being obtained in the same animal and of showing the entire global extent, which is not possible to obtain with other methods (Xu et al, 2000). We have pointed out the advantages of the olfactory bulb in analysing the relation between activity and metabolic requirements underlying fMRI imaging in the brain (Shepherd, 2003).

Study 5. Complex processing by neuronal dendrites in the olfactory bulb. The information contained in the odor maps is processed by the microcircuits of the olfactory bulb. These microcircuits are largely formed by the dendrites of mitral/tufted cells and their interactions with two types of interneuron: periglomerular (PG) cells and granule cells. Previously we have shown that the site of action potential initiation shifts dynamically dependent on levels of synaptic excitation and inhibition. To test this model further we have carried out a computational study, which has shown a novel "ping-pong" effect of the action potential initiation site shifting from distal to proximal dendrite under different conditions of synaptic excitation in the glomerulus and synaptic inhibition from the granule cells (Chen et al, 2002). Further analysis of the properties of the distal dendrites in the glomerular tuft have been carried out using Ca imaging combined with two-photon microscopy (Zhou et al, in preparation).

Mitral cells are also interconnected in their distal dendrites in the glomerulus by gap junctions which mediate electrical interactions between them. It has been postulated that this provides a mechanism for synchronization of mitral cells. Experimental evidence for synchronization has been obtained in recordings from mitral and periglomerular cells (Zhou et al, in preparation; Jia et al, in preparation). To test the gap junction hypothesis we have carried out computational studies, which have shown the operating range over which the gap junctions are likely to bring about synchronization. The study has also provided clear evidence of the critical role of the long primary dendrite in the integrative actions of the mitral cell, which need to be taken into account in the construction of neural networks of these and similar cortical cells. A report is in preparation (Migliore and Shepherd, in preparation).

Study 6. Neuronal functional phenotype depends on dendritic properties. The mitral/tufted cells, like other neuron types, have a distinctive morphology and mode of action potential firing. In order to gain insight into the relation between the morphological types and firing patterns we carried out a study to classify them. The tentative result was a flow diagram showing how different types of dendritic morphology and different types of firing patterns could be related to the different distributions of voltage-gagted ion channels in the dendrites by a hierarchical scheme (Migliore and Shepherd, 2003). Further studies will be needed to test this hypothesis.

Dr. James Bower:

Our subproject carried out several studies during the five years of the grant plus the final one year no-cost extension (overall 1998-2004). In general our efforts were focused on two main areas: physiological and modeling studies of the relationships between the periodic oscillatory behavior of the olfactory system and an effort to understand how humans classify and organize olfactory information.

A. Is there a natural order in olfactory stimuli?

Odor quality is thought to depend primarily on the chemical structure of the olfactory stimulus. In form, this hypothesis can be traced back to Lucretius, who in 50 BCE suggested that agreeable odors were produced when the olfactory system encountered "smooth" particles, while disagreeable, harsh odors were generated by "hooked" particles [1]. This idea was made more explicit in the early 20th century when Henning [2] linked odor classes to specific molecular features (as referenced in Schiffman [3]). Current thinking suggests that the olfactory system functions as a "chemical classifier", where olfactory perception is organized around the detection of different structural classes of molecules by different classes of receptor proteins (e.g., [4-7]). In support of this idea, the organizational principles governing molecules in organic chemistry have become, in practice, the favored hypothetical organizational principles for olfactory perception. Specifically, structural homology is implicitly used to explore odor "topography" in the olfactory system with most studies based on sets of chemical stimuli representing small changes in chemical structure between molecules with similar chemical properties (e.g., carbon chain length [8-10]). Thus homologous series of alcohols [8, 11-15], aldehydes [8, 11, 16, 17], and/or other simple organic molecules [18-20] are regularly used to examine the response properties of olfactory receptor molecules [20], olfactory receptor neurons [12], bulbar [11, 16, 19] and cortical [20] neuronal responses, as well as psychophysical responses to these stimuli [8, 13-15].

While probing the olfactory system with homologous series of odorants is standard across a wide range of studies, the results obtained usually indicate some more complex pattern of organization. Thus, for example, studies of single olfactory receptor binding properties indicate that while individual receptors might bind to two to three consecutive molecules in a series, molecules taken from other series also often elicit responses [20]. More generally, psychophysical analysis of odor perception demonstrates that similarity in molecular structure does not also predict similarity in odor quality, an observation consistently observed for almost half a century [21]. In fact, it is still not possible to predict the odor quality elicited by a stimulus based on molecular structure alone [3]or even to know for certain that a particular molecule will elicit an odor at all. Finally, the strongest argument that the organization of odor perception is not based simply on structural homology is that a change in the concentration of the same monomolecular stimulus can produce dramatic changes in its elicited odor [22]. Thus, it is clear that the olfactory system is doing something more complex than merely detecting different molecules based on their chemical structure.

In this paper we report the results of an effort that initially disregarded the chemical structure of odorants, and instead sought evidence of order in the relationships between odor perceptions, and subsequently whether a similar order might exist in the organization of olfactory stimuli. First,

using two large published data sets of odor descriptors elicited by different monomolecular stimuli [23, 24], we have used a cross-entropy analysis of the co-occurrence of pairs of descriptors associated with different molecules, to generate directed graphs representing the relationships between these descriptors. We have found that both datasets, generated by different olfactory specialists, are quite similar. Second, we have further analyzed these graphs with respect to molecules known to elicit different odor perceptions with varied concentration. This analysis has revealed that all tested molecules of this class fall into one of three transitions in the graph. Finally, when the molecular structure of the molecules whose descriptors also map to these graph locations are analyzed, we discovered that the entire graph can be divided into regions whose descriptors represent molecules containing sulfur, nitrogen or carbon. We interpret this result to imply that olfactory perception reflects some understanding of different biogenetic pathways in the natural world, rather than the kind of organization suggested by structural chemical homology. This hypothesis has important implications for the interpretation of studies of the structure and specificities of olfactory receptors as well as investigations of structure-function relationships in olfactory systems as a whole.

References

1. Lucretius, On the Nature of Things. 50 BC.
2. Henning, H., Der Geruchs. 1912, Leipzig.
3. Schiffman, S.S., Contributions to the physicochemical dimensions of odor: a psychophysical approach. Ann. NY Acad. Sci., 1974. 237: p. 164-183.
4. Belluscio, L. and L.C. Katz, Symmetry, stereotypy, and topography of odorant representations in mouse olfactory bulbs. Journal of Neuroscience, 2001. 21(6): p. 2113-2122.
5. Johnson, B.A., et al., Functional mapping of the rat olfactory bulb using diverse odorants reveals modular responses to functional groups and hydrocarbon structural features. Journal of Comparative Neurology, 2002. 449(2): p. 180-194.
6. Meister, M. and T. Bonhoeffer, Tuning and topography in an odor map on the rat olfactory bulb. Journal of Neuroscience, 2001. 21(4): p. 1351-1360.
7. Wilson, D.A., Receptive Fields in the Rat Piriform Cortex. Chem. Senses, 2001. 26: p. 577-584.
8. Laska, M. and P. Teubner, Olfactory discrimination ability for homologous series of aliphatic alcohols and aldehydes. Chem. Senses, 1999. 24(3): p. 263-270.
9. Wilson, D.A., Odor specificity of habituation in the rat anterior piriform cortex. J. Neurophysiol., 2000. 83: p. 139-145.
10. Uchida, N., et al., Odor maps in the mammalian olfactory bulb: domain organization and odorant structural features. Nat. Neurosci., 2000. 3(10): p. 1035-1043.
11. Imamura, K., N. Mataga, and K. Mori, Coding of odor molecules by mitral tufted cells in rabbit olfactory bulb .1. aliphatic-compounds. J. Neurophysiol., 1992. 68(6): p. 1986-2002.
12. Sato, T., et al., Tuning Specificities To Aliphatic Odorants In Mouse Olfactory Receptor Neurons And Their Local-Distribution. J. Neurophysiol., 1994. 72(6): p. 2980-2989.
13. Commetto-Muniz, J.E. and W.S. Cain, Relative Sensitivity Of The Ocular Trigeminal, Nasal Trigeminal And Olfactory Systems To Airborne Chemicals. Chem. Sens., 1995. 20(2): p. 191-198.

14. Laska, M., et al., Olfactory discrimination ability and odor structure-activity relationships in honeybees. Chem. Senses, 1999. 24(4): p. 429-438.
15. Laska, M., S. Trolp, and P. Teubner, Odor structure-activity relationships compared in human and nonhuman primates. Behavioral Neuroscience, 1999. 113(5): p. 998-1007.
16. Kashiwadani, H., et al., Synchronized oscillatory discharges of mitral/tufted cells with different molecular receptive ranges in the rabbit olfactory bulb. J. Neurophysiol., 1999. 82(4): p. 1786-1792.
17. Commetto-Muniz, J.E., W.S. Cain, and M.H. Abraham, Nasal pungency and odor of homologous aldehydes and carboxylic acids. Exp. Brain Res., 1998. 118(2): p. 180-188.
18. Mori, K., N. Mataga, and K. Imamura, Differential specificities of single mitral cells in rabbit olfactory bulb for a homologous series of fatty-acid odor molecules. J. Neurophysiol., 1992. 67(3): p. 786-789.
19. Johnson, B.A., et al., Multidimensional chemotopic responses to n-aliphatic acid odorants in the rat olfactory bulb. J. Comp. Neurol., 1999. 409(4): p. 529-548.
20. Malnic, B., et al., Combinatorial receptor codes for odors. Cell, 1999. 96(5): p. 713-723.
21. Harper, R., E.C. Bate Smith, and D.G. Land, Odour Description and Odour Classification. 1968, London: J.& A. Churchill.
22. Fenaroli, G., Fenaroli's Handbook of Flavor Ingredients. 2nd ed, ed. T.E. Furia and N. Bellanca. Vol. 2. 1975, Cleveland, OH: CRC Press.

B. Relations between sniffing and oscillations in olfactory cortex

While it has been known for many years that the nervous system generates oscillatory behavior in a wide range of frequencies (Adrian 1942, Freeman 1960, Bressler 1990, Steriade 1997), the functional significance of this dynamical behavior has recently become a growing focus for many physiologists (Engels and Singer 2001), modelers, and theorists. The oscillatory behavior of cerebral cortex and its associated structures in particular is now regarded by many as being directly linked to function (Engels, 2001). Current speculations on these functions range from the coding of sensory information (Singer and Gray 1995), to a substrate for attention (Fries 1997, Tiitinen 1993, Tallon-Baudry 1999), awareness and conciousness (Engels and Singer 2001, Sauve 1999, Crich and Koch 1990).

Central in many interpretations of the functional significance of cerebral cortical oscillatory behavior is the question of the origins of this behavior, and, in particular, its relationship to afferent input. Modeling efforts, including our own (Wilson and Bower 1992), together with experimental works (Sanchez-Vives and McCormick 1999), have suggested that the tendency of cortical networks to oscillate is an intrinsic property of both its networks and neurons (Wilson and Bower 1992, Hasselmo 2001). Others have observed that oscillatory patterns could be "driven" by deeper brain structures like the thalamus (Steriade, Destexhe) and that, under specific conditions, they could be related to sensory inputs (Ferster). Additional confusion in the literature results from the fact that the cerebral cortex generates many different frequencies of behavior, and it is often unclear how the oscillations described by one laboratory, relate to the oscillations described by another.

In several studies funded by the MURI and now complete, we have focused on oscillations in the olfactory system occurring at frequencies less than 1.5 Hz. These low frequency oscillations have been recorded here under conditions of ketamine/xylazine anesthesia and are comparable to similar slow oscillations observed in neocortical areas by Steriade and colleagues using the same anesthetic protocol (Steriade 1993 a, b). Based on similarities between these oscillations and those seen during slow wave sleep (SWS), Steriade has proposed that the presence of these slow oscillations reflects a behavioral condition in which the brain is mostly closed to the external environment and running on its own (Steriade 2000, Timofeev 1996). This assertion is consistent with electrophysiological results demonstrating slow wave oscillations in neocortical slices (Sanchez-Vives 2000) and slabs (Timofeev 2000) which, of course, are devoid of afferent sensory input. Recently similar oscillations have also been shown to occur in thalamic slices lacking afferent input (Hughes 2002),

We have used this ketamine/xylazine preparation to investigate the relationship between slow oscillations in primary olfactory (piriform) cortex and the presence of oscillatory activity in its afferent inputs. Unlike sensory neocortex in fact the overall temporal pattern of afferent inputs to the olfactory cortex is rhythmical and controlled by the sniffing (bressler, others). Using intracellular and extracellular recording techniques, we demonstrate here for the first time the presence of ketamine/xylazine-induced slow oscillations in membrane potential and local field potentials recorded in vivo from piriform cortex. Further we show that the occurrence of these neuronal activity patterns is directly correlated with the natural breathing cycle of the rat, and therefore is likely to be directly related to periodic patterns of afferent input linked to respiration. In supporting to this interpretation we demonstrate a considerable reduction in the amplitude and regularity of oscillations when air bypasses the olfactory system in tracheotomized preparations. Pulsing air into the nostrils in this preparation restores the oscillations, and can directly entrain their frequency. We therefore conclude that there is a direct relationship between slow oscillations in the olfactory cortex and in its sensory input. The conclusion that respiration is reflected in the temporal behavior of piriform cortex is also consistent with studies conducted as part of this larger research project in the olfactory bulb of rats (Sobel 1993) and with recent imaging results in humans (Sobel 1998).

We have previously suggested, based on computational grounds, that the fundamental neuronal architecture of cerebral cortex may have first evolved in the context of the olfactory system and then been adapted to the use of other sensory systems through the evolution of neocortex (Bower, 1995). We have speculated that the presumed general usefulness of the type of associative learning necessary for object recognition in the olfactory system drove this subsequent development of neocortex. As a consequence, however, we suggest that neocortex was forced to accept dynamical patterns of behavior more clearly related to olfaction than somatosensation, vision, audition, etc. We believe similarities in the neo and olfactory cortical mechanisms for the higher frequency theta (7-12 Hz) and gamma (30-50 Hz) oscillations revealed by our realistic modeling efforts (Wilson and Bower, 1991; 1992), support this point of view. With respect to the slow frequency behavior studied here, because the olfactory system is fundamentally linked to the metabolic function of respiration, air continues to move across the olfactory epithelium during the sleep state providing an ongoing periodic input. In neocortex, in contrast, sleep is associated with sensory deafferentation through the action of the thalamus whose decoupled neurons in the awake state become coupled, modulating slow wave activity in

the sleep state (Bazhenov, 2002). We suggest that these slow wave thalamic oscillations functionally correspond to the slow periodic activity generated by the rhythmic slow breathing associated with sleep in mammals. The essential point, and prediction is that proper function of cortical circuitry during sleep, whatever that function is (Wilson and McNaughton, 1993; Lee and Wilson, 2002), requires or expects such slow periodic input because of an evolutionary link between cortical circuitry and olfaction. It remains to be seen whether there is any specific temporal relationship between rhythmic breathing during sleep, and the timing of slow oscillations in the thalamus and neocortex.

References

1 Adrian ED (1942) Olfactory reactions in the brain of the hedgehog. J Physiol (Lond) 100:459-473.

2 Bhalla US, Bower JM (1997) Multiday recordings from olfactory bulb neurons in awake freely moving rats: spatially and temporally organized variability in odorant response properties. J Comput Neurosci 4:221-256.

3 Biella GR, Dickson CT, De Curtis M, (2001) Slow periodic activity in rhinal cortices of the isolated guinea pig brain preparation. Soc Neurosci Abstr 27:847.14

4 Bower JM (1995) Reverse engineering the nervous system: an in vito, in vitro, and in computo approach to understanding the mammalian olfactory system. In: An Introduction to Neural and Electronic Networks, Second Edition. S. Zornetzer, J. Davis, and C. Lau, editors. Academic Press. pp. 3-28.

5 Bremer F (1958) Cerebral and cerebellar potentials. Physiol Reviews 38:357-388

6 Bressler SL, Freeman WJ. Frequency analysis of olfactory system EEG in cat, rabbit, and rat. (1980) Electroencephalogr Clin Neurophysiol. 50:19-24

7 Bressler SL (1984) Spatial organization of EEGs from olfactory bulb and cortex. Electroencephalogr Clin Neurophysiol 57:270-276.

8 Buzsaki G (1998) Memory consolidation during sleep: a neurophysiological perspective. J Sleep Res 7:17-23.

9 Carandini M, Ferster D (2000) Membrane potential and firing rate in cat primary visual cortex. J Neurosci 20:470-484.

10 Chaput MA, Buonviso N, Berthommer F (1992) Temporal patterns in spontaneous and odour-evoked mitral cell discharges recorded in anesthetized freely breathing animals. Eur J Neurosci 4:813-822.

11 Chaput MA (2000) EOG responses in anesthetized freely breathing rats. Chem Senses 25:695-701

12 Collins ER, Lang EJ, Pare D (1999) Spontaneous activity of the perirhinal cortex in behaving cats. Neuroscience 89:1025-1039.

13 Collins DR, Pelletier JG, Pare D (2001) Slow and fast (gamma) neuronal oscillations in the perirhinal cortex and lateral amygdala. J Neurophysiol 85:1661-1672.

14 Destexhe A., Sejnowski T.J., (2001), Thalamocortical assemblies, Monographs of the Physiological Society (49), New York: Oxford UP.

15 Engel AK, Fries P, Singer W (2001) Dynamic predictions: oscillations and synchrony in top-down processing. Nat Rev Neurosci 2:704-716

16 Fontanini A, Vanier MC, Moore LE, Bower JM (2001) Membrane potential oscillations in piriform cortex pyramidal cells: *in vivo* intracellular and local field potential recordings. Soc Neurosci Abstr 27:726.5.

17 Freeman WJ (1959) Distribution in time and space of prepyriform electrical activity. J Neurophysiol 22:644-665.

18 Freeman WJ (1960) Correlation of electrical activity of prepyriform cortex and behavior in cat. J Neurophysiol 23:111-131

19 Freeman WJ (2000) Neurodynamics: an exploration in mesoscopic brain dynamics. London: Springer.

20 Haberly LB (1973) Unitary analysis of opossum prepyriform cortex. J Neurophysiol 36:762-774

21 Haberly LB, Bower JM (1984) Analysis of association fiber system in piriform cortex with intracellular recording and staining techniques. J Neurophysiol 51:90-112.

22 Haberly LB (1990) Comparative aspects of olfactory cortex. In: Cerebral cortex (Jones EG and Peeters A eds), pp 137-166. New York: Plenum

23 Haberly L.B., (1998), Olfactory Cortex. In: The synaptic organization of the brain. (Shepherd GM, ed), pp 377-416. New York: Oxford UP.

24 Hasselmo ME, Fransen E, Dickson C, Alonso AA (2000) Computational Modeling of Entorhinal Cortex. Ann N Y Acad Sci 911:418-446

25 Hopfield JJ (1995) Pattern recognition computation using action potential timing for stimulus representation. Nature 376:33-36.

26 Ketchum K.L., Haberly L.B (1993), Membrane currents evoked by afferent fiber stimulation in rat piriform cortex. I. Current source-density analysis, J. Neurophysiol 69:248-260.

27 Lee AK, Wilson MA. (2002) Memory of Sequential Experience in the Hippocampus during Slow Wave Sleep. Neuron 36:1183-1194

28 Macrides F., Chorover S.L. (1972) Olfactory bulb units: activity correlates with inhalation cycles and odor quality. Science 175:84-87.

29 Paxinos G, Watson C (1997) In: The rat brain in stereotaxic coordinates, Ed 3. San Diego: Academic.

30 Sanchez-Vives MV, McCormick DA (2000) Cellular and network mechanisms of rhythmic recurrent activity in neocortex. Nat Neurosci 3:1027-1034.

31 Sobel EC, Tank DW (1993) Timing of odor stimulation does not alter patterning of olfactory bulb unit activity in freely breathing rats. J Neurophysiol 69:1331-1337.

32 Sobel N, Prabhakaran V, Desmond JE, Glover GH, Goode RL, Sullivan EV, Gabrieli JD (1998) Sniffing and smelling: separate subsystems in the human olfactory cortex. Nature 392:282-286.

33 Steriade M, Nunez A, Amzica F (1993a) A novel slow (< 1 Hz) oscillation of neocortical neurons in vivo: depolarizing and hyperpolarizing components. J Neurosci 13:3252-3265

34 Steriade M, Nunez A, Amzica F (1993b) Intracellular analysis of relations between the slow (< 1 Hz) neocortical oscillation and other sleep rhythms of the electroencephalogram. J Neurosci 13:3266-3283.

35 Steriade M (1997) Synchronized activities of coupled oscillators in the cerebral cortex and thalamus at different levels of vigilance. Cereb Cortex 7:583-604

36 Steriade M (2000) Corticothalamic resonance, states of vigilance and mentation. Neuroscience 101:243-276

37 Steriade M, Timofeev I, Grenier F (2001) Natural waking and sleep states: a view from inside neocortical neurons. J Neurophysiol 85:1969-1985

38 Stripling JS, Patneau DK (1999) Potentiation of late components in olfactory bulb and piriform cortex requires activation of cortical association fibers. Brain Res 841:27-42

39 Timofeev I, Contreras D, Steriade M (1996a) Synaptic responsiveness of cortical and thalamic neurones during various phases of slow sleep oscillation in cat. J Physiol 494:265-278

40 Timofeev I, Steriade M (1996b) Low-frequency rhythms in the thalamus of intact-cortex and decorticated cats. J Neurophysiol 76:4152-4168.

41 Timofeev I, Grenier F, Bazhenov M, Sejnowski TJ, Steriade M. Origin of slow cortical oscillations in deafferented cortical slabs.(2000) Cereb Cortex 10:1185-1199.

42 Traub R.D., Jeffreys G.R., Whittington M.A. (1999), Fast oscillations incortical circuits, Cambridge, MA: MIT Press.

43 Tsubone H (1990) Nasal 'pressure' receptors. Nippon Juigaku Zasshi 52:225-232

44 Wehr M, Laurent G (1996) Odour encoding by temporal sequences of firing in oscillating neural assemblies. Nature 384:162-166

45 Wilson D (1998) Habituation of odor responses in the rat anterior piriform cortex. J Neurophysiol 79:1425-1440

46 Wilson M, Bower JM (1992) Cortical oscillations and temporal interactions in a computer simulation of piriform cortex. J Neurophysiol 67:981-995

47 Wilson MA and Bower JM (1991) A computer simulation of oscillatory behavior in primary visual cerebral cortex. Neural Computation 3: 498-509

48 Wilson MA, McNaughton BL (1994) Reactivation of hippocampal ensemble memories during sleep. Science 265:676-679

Dr. Linda Buck:

A. Combinatorial receptor codes for odors

In one part of this project, we asked how odorant receptors (ORs) in the nose encode the identities of a vast array of environmental chemicals. Mice have ~1000 different ORs, each expressed by a different subset of olfactory sensory neurons (OSNs) in the nose. Although the ORs were identified in 1991, little was known about the odorants recognized by individual ORs because it was not possible to functionally express ORs in heterologous cells where their functions could be tested. To circumvent this problem, we developed an alternative strategy in which we first used calcium imaging to identify mouse OSNs responsive to individual odorants and then single cell reverse transcriptase (RT)-PCR to identify the OR genes expressed in those neurons.

In initial studies, we asked whether individual OSNs actually do express only one OR gene, as predicted. In our experiments we used a two step RT-PCR protocol. In the first step we prepared and amplified cDNAs matching all (or most) mRNAs in the neuron. In the second step, we used OR primers to amplify cDNAs from an aliquot of the first PCR reaction. Using degenerate primers matching conserved sequence motifs in mammalian ORs, we identified OR genes expressed in >50 single OSNs in these and other experiments. In every case, we identified only one expressed OR per neuron. We also performed a number of control experiments to further investigate not only the number of OR genes expressed per OSN, but also the ability of our single cell RT-PCR method to accurately identify the OR genes expressed in individual OSNs. The following results provided strong evidence that each OSN expresses only one OR gene:

1. OR cDNAs obtained from the same OSN with different primers were identical in overlapping regions.

2. All 60 cloned OR cDNAs derived from the same neuron hybridized to the same OR probe in each case tested.

3. When total cDNAs amplified from pairs of cells were mixed and then subjected to PCR with OR primers, the OR cDNAs obtained from each alone were present, indicating that more than one OR cDNA could be detected if present.

4. When the first strand cDNAs made from individual neurons were split into 3 tubes and then subjected to the two step PCR protocol, the OR cDNAs amplified from the 3 tubes were identical, excluding the possibility that the ORs detected with our method derive from contaminating genomic DNA (since there are only two alleles of each gene).

For test odorants, we used a series of aliphatic odorants with straight carbon chains ranging in length from 4 to 9 carbon atoms. We used four different classes of aliphatic odorants with the same carbon chains, but different functional groups: carboxylic acids, aliphatic alcohols, bromocarboxylic acids, and dicarboxylic acids. Only a small percentage of neurons (0-7% of >600 neurons tested) responded to individual test odorants.

We identified ORs expressed in 14 neurons responsive to the test odorants. Since each neuron expressed only one OR gene, the response profile of the neuron indicated the recognition profile of the OR it expressed. Consistent with previous functional studies of OSNs, we found that individual ORs can recognize multiple odorants. Our results also showed that a single odorant can be recognized by multiple ORs. Importantly, however, different odorants were recognized by different combinations of ORs. Thus the identities of different odorants are encoded by different combinations of receptors. This combinatorial use of the OR family should allow, in principle, for an ability to detect and discriminate an enormous variety of odorants whose number vastly exceeds that of ORs. Even if each odorant were encoded by only three receptors, this combinatorial coding scheme would generate almost one billion different odor codes.

Our studies also showed that there is tremendous diversity in the recognition properties of different ORs. Both the carbon chain length of the odorants and their functional groups were important for recognition for most of the ORs we identified, but the combinations of carbon chain lengths and functional groups that could be recognized, or tolerated, by individual receptors varied tremendously. In addition, we found that a single odorant can be recognized by both highly related and divergent ORs.

In addition, these studies showed that even a slight change in the structure of an odorant, or a change in its concentration, can change its "receptor code", the combination of ORs that recognize the odorant. This suggests that changes in receptor code may underlie perceptual alterations in humans that can result from changes in odorant structure or concentration.

In summary, our studies indicate that the olfactory system uses a combinatorial receptor coding scheme to distinguish odors. In this scheme, the identities of different odorants are specified by different combinations of receptors, but each receptor can be used as one component of the codes for many odors. This scheme explains how 1000 different receptors can allow for the discrimination of thousands or tens of thousands of different odors in the external environment.

B. Detection of odorants and pheromones by the vomeronasal organ

In addition to odorants, the olfactory system detects pheromones, chemicals released from animals that stimulate hormonal changes or specific behaviors, such as mating or aggression, in members of the same species. Many mammals have a second olfactory sense organ, the vomeronasal organ (VNO), which is thought to be specialized to detect pheromones. In previous studies, we and others found that the VNO and nose use different mechanisms to detect sensory ligands. Two distinct families of receptors are expressed in the VNO, the V1R and V2R families, and the different families are expressed by different subsets of VNO neurons. As in the nose, however, it appears that each neuron expresses only one receptor gene.

To determine how the VNO system encodes sensory information, we used calcium imaging to analyze responses of single mouse VNO neurons to pheromones. We also examined responses of these neurons to odorants.

We found that, similar to OSNs, VNO neurons exhibit transient increases in intracellular calcium when they are exposed to 140mM KCl. These increases are likely to be due to influx of calcium through voltage-sensitive calcium channels that open upon membrane depolarization by KCl.

In initial studies, we tested VNO neurons for responsiveness to six different mouse pheromones: dehydro-exo-brevicomin, 2,5-dimethylpyrazine, E-beta-farnesene, 2-heptanone, lactol (6-hydroxy-6-methyl-3-heptanone), and 2-sec butyl-4,5-dihydrothiazole. The pheromones were tested at 100uM except for dehydro-exo-brevicomin (7uM), 2,5-dimethylpyrazine (1uM) and 2-sec butyl-4,5-dihydrothiazole (7uM), because of limited supplies when the experiments were done. In later studies supported by the NIH, we tested additional neurons with these pheromones as well as with odorants. Interestingly, individual pheromones elicited responses in only about 0.3-0.7% of VNO neurons. Given that there are about 260 different types of VNO receptors, this raises the possibility that some pheromones may be detected by only a single receptor type rather than by a combination of receptors as in the nose. Surprisingly, we found that VNO neurons can also detect some odorants, but not all. Given the neural pathway followed by signals generated in the VNO, this raises the possibility that some odorants may also be capable of stimulating hormonal changes or instinctive behaviors in mice.

C. The human OR gene repertoire

In the later part of this project, we characterized the human OR family. To identify human OR genes, we searched the NCBI finished and unfinished human genome sequence databases. In these searches, we used as queries either short amino acid sequence motifs conserved among mammalian ORs or a diverse set of mouse ORs. With these queries, we searched for related sequences in all 6 possible translated reading frames of the human genome sequence. We then isolated the DNA sequence surrounding each match and translated it to determine the encoded protein. Classification as an OR gene was based on visual inspection and, in some cases, by searching the NCBI protein database with the translated gene.

In these studies, we identified 339 intact OR genes and 297 OR pseudogenes in the human genome. Since the genome sequence was ~93% complete at the time we did this work, this is likely to represent the full, or nearly full, repertoire of human ORs.

We next determined the chromosomal location of each human OR gene. We did this by examining the chromosomal assignment of the clone in which each gene was found. Remarkably, we identified 51 different OR gene loci. We found OR gene loci on every human chromosome except chromosome 8 and the Y chromosome, a total of 21 different chromosomes.

OR genes can be divided into subfamilies on the basis of sequence relationships. Previous studies support the idea that closely related OR genes that belong to the same subfamily may encode receptors that recognize structurally-related odorants. Using a cutoff of 60% nucleotide sequence identity to define members of the same subfamily, the intact human ORs assorted into 172 different subfamilies. We found that members of the same subfamily are usually found at the same chromosomal locus. This raises the possibility that different OR gene loci might have different functions in odorant recognition.

It has been proposed that humans may be relatively defective in olfactory perception compared to mice and rats. This idea was based on preliminary indications that mice may have more OR genes than humans. In other studies, which were supported by the NIH, we analyzed the mouse OR gene repertoire. Comparison of human and mouse OR families showed that mice have about 2.7 times as many ORs as humans and 241 OR subfamilies compared to the 172 found in human. When we performed a detailed comparison of human and mouse ORs, we found that most human OR subfamilies are found in mouse. Interestingly, however, the mouse subfamilies almost invariably have more member ORs. This suggests that humans and mice are likely to detect many of the same odorant structural features, but that mice may have a superior ability to discriminate odorants with highly related structures.

Dr. Noam Sobel:

The process whereby an odorant (physical entity) becomes a smell (percept) consists of several stages. Initially, the odorant must be sniffed into the nasal passage. This crucial initial stage of olfactory processing is often overlooked. Following this sampling phase, the odorants are transduced by receptors ligning the olfactory epithelium. The transduced information is then processed first at the level of olfactory bulb, and later olfactory cortex. This MURI investigated olfactory processing **from Detection to Classification**, and our lab contributed to the study of both processes:

Odorant detection -- Sampling

Sniffs are modulated in response to odor content. Higher concentrations of odor induce lesser-volume sniffs. This phenomenon implicates a neural feedback mechanism that measures sensory input (odor concentration) and modulates motor output (sniffing) accordingly[1,2]. We are interested in this modulatory mechanism both in order to better understand the olfactory process, and to explore the implementation of such a mechanism in artificial olfactory devices (electronic noses). We therefore first set out to ask what are the temporal parameters of this mechanism. A stainless-steel computer-controlled olfactometer, equipped with mass flow controllers, temperature and humidity control, and on-line photo-ionization detection, was coupled to a highly sensitive pneumatotachograph that measured nasal flow. The olfactometer was used to generate four ascending concentrations of the odorants propionic acid and phenethyl alcohol. We found that sniff volume was inversely related to odor concentration ($p < 0.0001$). Furthermore, sniffs were uniform and concentration-independent for the initial 150 msec, but acquired a concentration-dependent flowrate as early as 160 msec following sniff onset for propionic acid ($p < .05$), and 260 msec for phenethyl alcohol ($p < .05$). We published these results in the MURI-supported manuscript by Johnson et al[3].

These findings are important, firstly because they merit reframing our view of the temporal aspects of olfaction. Olfaction is traditionally considered a "slow" sensory process. Our results suggest otherwise, and point to rapid processing in olfaction. These results also raise important questions regarding olfactory sensory transduction. The current view is that odorant transduction takes around 150 ms[4,5]. However, the sniff-modulation that we see within 160 ms, renders the 150 ms value unlikely (it is unreasonable that the modulation would be achieved within 10 ms). Our finding of rapid processing has now also been replicated in rats[6], suggesting that the temporal dynamics of transduction should be revisited and revised.

Furthermore, the rapid olfactomotor function we have characterized suggests that olfactomotor sniff feedback control is subcortical and may rely on neural mechanisms similar to those that modulate eye movements to accommodate vision and ear movements to accommodate audition. We have now embarked on localizing this mechanism in the brain, and have some evidence suggesting that it may be cerebellar.

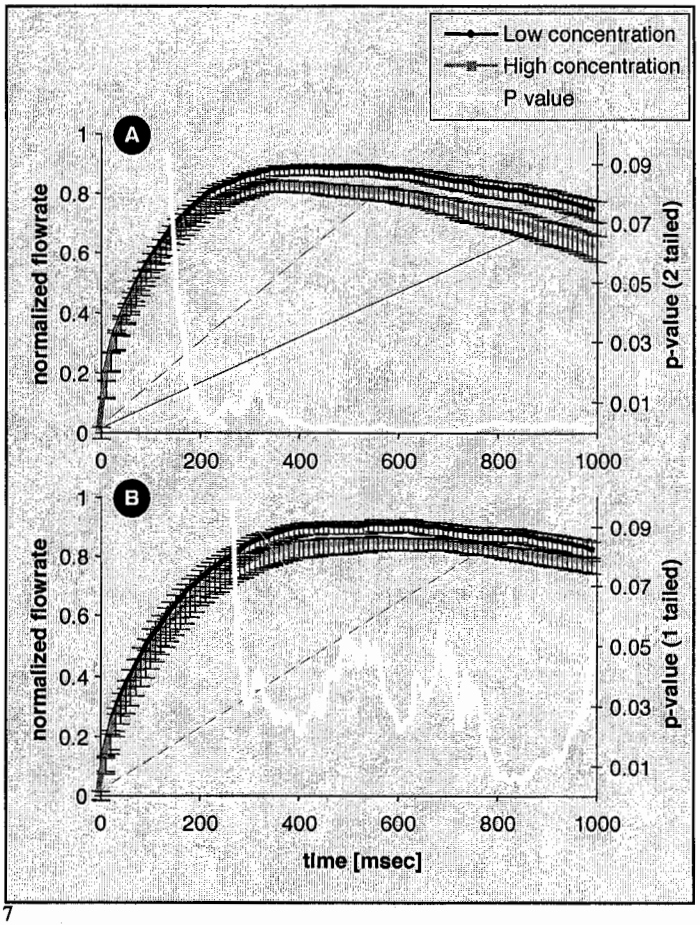

7

Figure 1. First second of the mean sniff to low and high concentrations of a) propionic acid, b) phenethyl alcohol. The blue line is the mean sniff to low concentration, and the red line is the mean sniff to high concentration. Bars are standard error. The p-value from the associated paired t-test is shown in yellow. Sniffs of propionic acid are significantly concentration dependent by 160 msec, and sniffs of PEA are significantly concentration dependent by 260 msec.

Odorant detection -- Specific anosmia

The olfactory system is a model for neural plasticity in that its sensory neurons and connectivity are continuously renewed throughout life[8]. An example of plasticity in the adult human olfactory system is learned detection of androstenone (5 alpha-androst-16-en-3-one). Approximately 30% of the adult human population does not perceive an odor when sniffing the steroidal compound androstenone, but such sensitivity can be induced by repeated exposure[7]. To understand the mechanisms of plasticity underlying this acquired capability, one must first determine its location in the olfactory system. Is plasticity occurring peripherally at the olfactory receptors in the nose, or centrally in the brain? To address this question we systematically exposed only one nostril of androstenone non-detectors to androstenone and then tested the unexposed, naive, nostril. Considering that the two olfactory pathways are not neurally connected at the peripheral level, if the naive nostril had learned to detect androstenone, this would suggest that plasticity occurred centrally. By contrast, if the naive nostril remained unable

to detect androstenone while the exposed nostril learned, this would suggest that plasticity occurred peripherally.

We screened 42 subjects for androstenone detection using a four-trial, three-alternative-forced-choice paradigm with criteria set at two or fewer correct trials. This screen yielded 12 non-detectors, a prevalence of non-detection (29%) equivalent to that in previous reports. These non-detectors returned to the lab for ten-minute sessions daily, for 21 days, where one nostril was continuously exposed to androstenone. The other nostril was blocked by insertion of an inflatable plug. Five liters per minute of heated, humidified, bottled air were injected through the plug to prevent any androstenone from entering the occluded nostril by reverse flow (retronasal olfaction). At the beginning of the experiment this group was at 25% accuracy (SD=11%), which is not significantly different from 33% chance (Binomial from chance: $p = .9$). Twenty-one days of exposure doubled androstenone detection accuracy in the exposed (change from baseline: $t(11) = 3.3$, $p < .007$. Binomial from chance: $p < .002$), and unexposed (change from baseline: $t(11) = 2.3$, $p < .04$. Binomial from chance: $p < .02$) nostrils respectively (Fig. 2). There was no significant difference in the extent of improvement between the exposed and unexposed nostrils ($t(11) = .4$, $p = .7$). This finding indicates that the site of plasticity underlying learned detection of androstenone communicates with both nostrils via a central component. We published these results in the MURI-supported manuscript by Mainland et al[9]

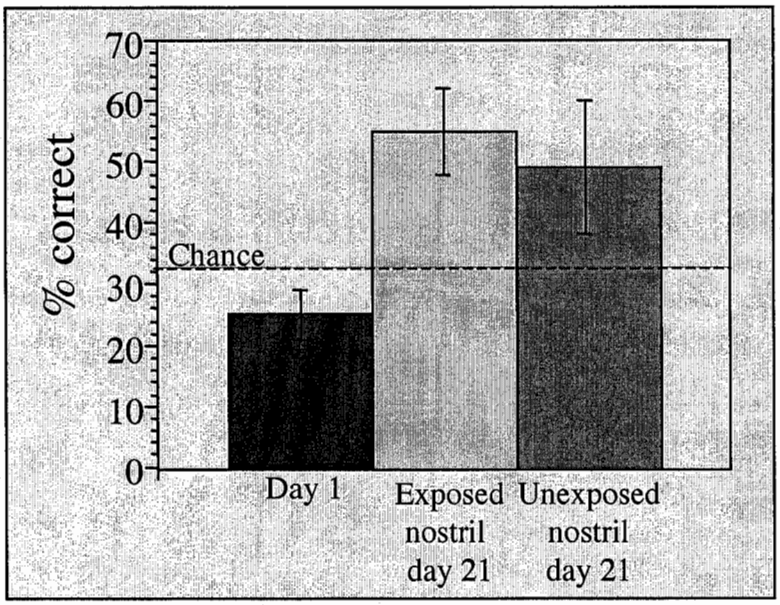

Figure 2. Detection accuracy at pre-exposure and in the exposed and unexposed nostrils following 21 days of exposure.

We took advantage of the paired anatomy of the olfactory system to find that the plasticity underlying the emergence of androstenone detection has a central component. Such a component may be likened to pattern recognition. Despite the equivalent retinal image, a CT scan may appear all gray to the layperson while revealing intricate anatomy to the trained neurologist. Similarly, the nose may have been delivering the same signal to the brain at the beginning and end of this experiment, but through repeated exposure the brain may have learned to make sense of a previously senseless signal. Such learning may have occurred at the olfactory

bulbs or in primary olfactory cortex, a substrate that shares information from both nostrils[10] and is optimized for olfactory learning[11].

Odorant classification

Two aspects of odor that are encoded by the olfactory system are intensity (high/low) and valence (pleasant/unpleasant). These aspects are tightly linked. Most pleasant odorants become more pleasant as their intensity increases, and most unpleasant odorants become more unpleasant as their intensity increases[12]. Some odorants, such as indol and skatol, dramatically change their percept as intensity is varied. In other words, intensity is an axis of odorant classification. Here we used fMRI to ask if these tightly linked dimensions of intensity and valence are encoded by dissociable neural mechanisms. To dissociate the dimensions of intensity and valence, we devised four stimuli using two odorants. High and low concentration versions of the odorants citral and valeric acid were prepared. Citral smells lemony, fruity, and fragrant, and is perceived by most as pleasant[13]. Valeric acid smells sweaty, rancid, and sickening and is perceived by most as unpleasant[13]. The concentrations used were selected through a psychophysical prestudy where the high concentration citral was rated similar in intensity to the high concentration valeric acid, and the low concentration citral was rated similar in intensity to the low concentration valeric acid. Further, an intensity range was selected such that odor valence could be manipulated with relative independence from intensity. Thus, the above design provided four conditions [1. intense-pleasant 2. intense-unpleasant 3. unintense-pleasant 4. unintense-unpleasant] that allowed for a dissociation of intensity from valence (Fig. 3).

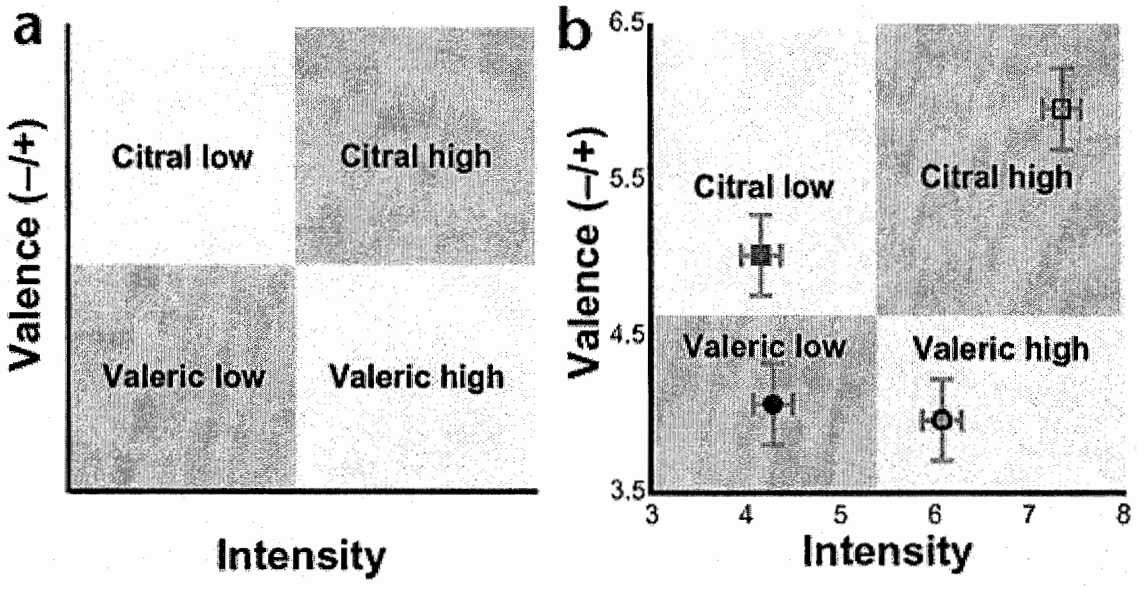

Figure 3: Ideal and observed odor space.
The abscissa represents odor intensity. The ordinate represents odor valence, with increasing pleasantness represented as greater magnitudes. (**a**) Odor selections were guided by an attempt to construct an affective space whereby odor intensity and valence were manipulated independently. High and low concentrations of the pleasant-smelling citral and unpleasant-smelling valeric acid were psychophysically pre-selected to represent the four critical design

quadrants. (**b**) Subjective intensity and valence estimates obtained after scanning. Horizontal error bars reflect standard error of the mean (s.e.m.) for intensity ratings from 1 (low intensity) to 9 (high intensity) and vertical reflects s.e.m. for valence from 1 (very unpleasant) to 9 (very pleasant). Consistent with the manipulation of odor valence, valeric acid was rated as significantly more unpleasant than citral ($F1,15 = 25.30$, $P< 0.0001$). Consistent with the manipulation of odor intensity, high-concentration odors were rated as significantly more intense than low-concentration odors ($F1,15 = 78.45$, $P< 0.0001$). Independent manipulation of intensity and valence was achieved for three of the four design quadrants; this was sufficient to separate neural responses to intensity and valence. Low concentrations of citral and valeric acid were equated for intensity ($F1,15 = 0.10$, $P> 0.75$), but differed in valence ($F1,15 = 6.46$, $P< 0.02$); high and low concentrations of valeric differed significantly in intensity ($F1,15 = 20.31$, $P< 0.0004$), but not in valence ($F1,15 = 0.08$, $P> 0.78$). High concentrations of citral were rated as more intense ($F1,15 = 10.25$, $P< 0.007$) than high concentrations of valeric, and more pleasant ($F1,15 = 7.68$, $P< 0.01$) than low citral. Consistent with their relative independence, there was no significant association between individuals' estimations of odor intensity and valence for both odorants (valeric, $r= -0.19$, $P> 0.27$; citral, $r= 0.29$, $P> 0.11$).

We delivered the four stimuli interspersed with a clean air stimulus in a random ordered event-related design to 16 participants while measuring brain activation with a 3 Tesla fMRI scanner. We found that amygdala activation was associated with intensity and not valence of odors. Conversely, distinct regions of orbitofrontal cortex were associated with valence independent of intensity (Figure 4). We published these results in the MURI-supported manuscript by Anderson et al[14].

Consistent with the sensory nature of odor intensity, in the olfactory system initial intensity coding occurs at the levels of the olfactory epithelium and bulb[15], and has been implicated at primary olfactory cortex[16,17], which includes the amygdala[18]. In contrast, our findings suggest that higher-order hedonic differentiation occurs in secondary olfactory regions, which include the orbitofrontal cortices[18]. Thus, the present results suggest a major division of the neural representation of affective space into more primary intensity and higher-order hedonic components. In contrast with relatively preserved hedonic responses in patients with amygdala lesions[19], it has been long known from stroke patients that the prefrontal cortices make important contributions to the experience of hedonic tone[20,21], with more recent studies highlighting specifically the critical role of the orbitofrontal cortices[21,22]. Such critical prefrontal contributions to hedonicity dovetail nicely with appraisal theories of human emotion that emphasize how affective responses are not simply a reflection of the intrinsic quality (positive vs. negative) of a stimulus, but result from interactions among the person, the situational context, and the stimulus[23]. Such flexibility of hedonic response is a hallmark of orbitofrontal representations, which are modulated by changes in affective relevance, as in the hungry versus sated state of the perceiver[24]. Thus, unlike the evolutionarily conserved functions of the amygdala, it appears that the malleability of human hedonic experience is characteristic of the more flexible, integrative, and evolved functions of the prefrontal cortices.

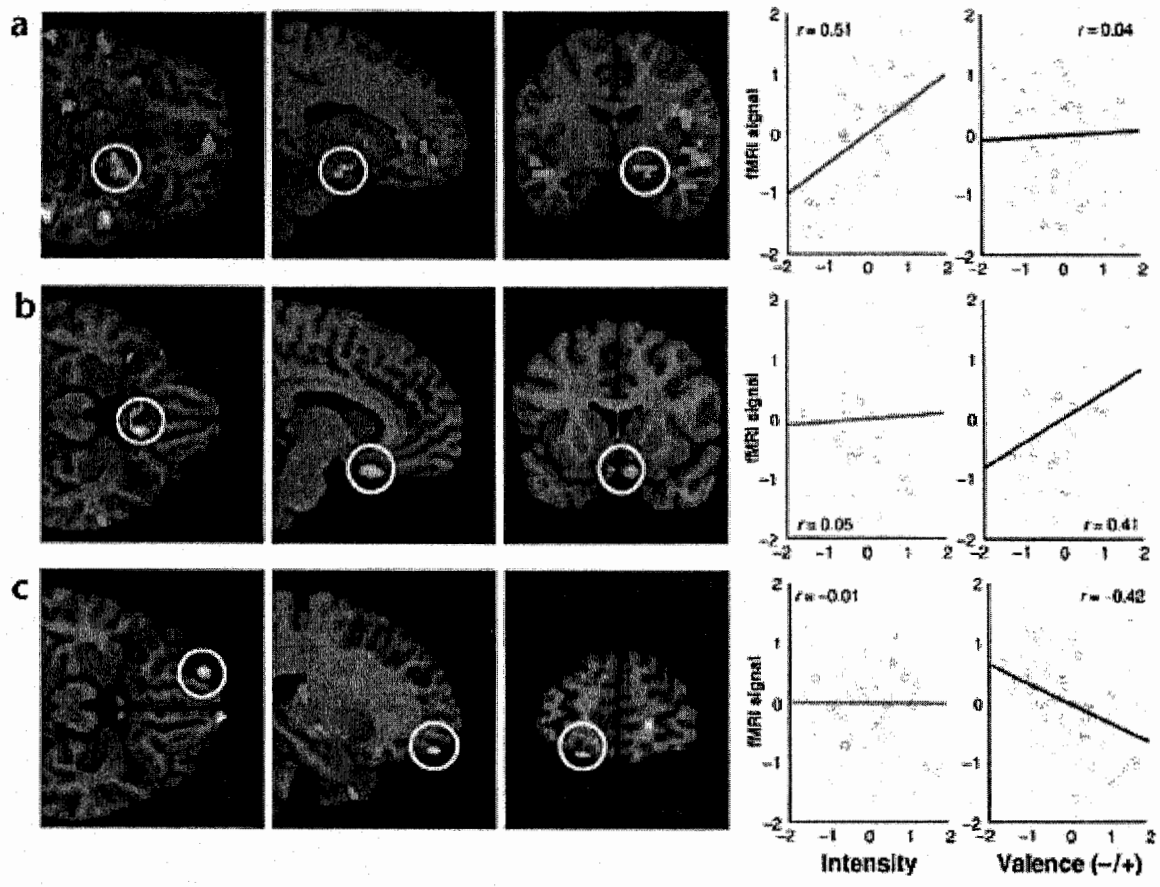

Figure 4: Functional regions of interest (fROI) defined by their correlation with individual differences either in the evaluation of intensity, pleasantness or unpleasantness of the four odor conditions and clean air.

Scatter plots depict the degree of association between individuals' fROI signal and valence and intensity evaluations (depicted as circles in standardized units). The ordinate represents fMRI signal, and the abscissa represents either the evaluation of odor intensity or valence for each stimulus condition for each participant. (**a**) A region in the right hemisphere extending from the dorsal amygdala into the piriform cortex was correlated with the evaluation of intensity but not valence. (**b**) A bilateral subcallosal gyrus activation extending into the posteromedial orbitofrontal cortex was correlated with the evaluation of pleasantness but not intensity. (**c**) Left anterior lateral and right anterior medial orbital cortical activations were correlated with the evaluation of unpleasantness but not intensity.

References

1. Laing, D. G. Natural sniffing gives optimum odour perception for humans. *Perception* **12**, 99-117 (1983).
2. Teghtsoonian, R., Teghtsoonian, M., Berglund, B. & Berglund, U. Invariance of odor strength with sniff vigor: an olfactory analogue to size constancy. *J Exp Psychol Hum Percept Perform* **4**, 144-52 (1978).

3. Johnson, B. N., Mainland, J. D. & Sobel, N. Rapid olfactory processing implicates subcortical control of an olfactomotor system. *J Neurophysiol* (2003).
4. Firestein, S. & Werblin, F. Odor-induced membrane currents in vertebrate-olfactory receptor neurons. *Science* **244**, 79-82 (1989).
5. Firestein, S., Shepherd, G. M. & Werblin, F. S. Time course of the membrane current underlying sensory transduction in salamander olfactory receptor neurones. *J Physiol* **430**, 135-58 (1990).
6. Uchida, N. & Mainen, Z. F. Speed and accuracy of olfactory discrimination in the rat. *Nat Neurosci* **6**, 1224-9 (2003).
7. Wysocki, C. J., Dorries, K. M. & Beauchamp, G. K. Ability to perceive androstenone can be acquired by ostensibly anosmic people. *Proc Natl Acad Sci U S A* **86**, 7976-8 (1989).
8. Graziadei, P. P., Levine, R. R. & Monti Graziadei, G. A. Plasticity of connections of the olfactory sensory neuron: regeneration into the forebrain following bulbectomy in the neonatal mouse. *Neuroscience* **4**, 713-27 (1979).
9. Mainland, J. D. et al. Olfactory plasticity: One nostril knows what the other learns. *Nature* **419**, 802 (2002).
10. Wilson, D. A. Receptive fields in the rat piriform cortex. *Chem Senses* **26**, 577-84 (2001).
11. Haberly, L. B. & Bower, J. M. Olfactory cortex: model circuit for study of associative memory? *Trends Neurosci* **12**, 258-64 (1989).
12. Doty, R. L. An examination of relationships between the pleasantness,.intensity and concentration of 10 odorous stimuli. *Perception and Psychophysiology*, 492-496 (1975).
13. Dravnieks, A. *Atlas of odor character profiles* (ASTM Press, PA, 1985).
14. Anderson, A. K. et al. Dissociation of the neural representations of intensity and valence in human olfaction. *Nat Neurosci* **6** (2003).
15. Duchamp-Viret, P., Duchamp, A. & Chaput, M. A. Peripheral odor coding in the rat and frog: quality and intensity specification. *J Neurosci* **20**, 2383-90 (2000).
16. Pause, B. M., Sojka, B. & Ferstl, R. Central processing of odor concentration is a temporal phenomenon as revealed by chemosensory event-related potentials (CSERP). *Chem Senses* **22**, 9-26 (1997).
17. Wilson, D. A. Binaral interactions in the rat piriform cortex. *J Neurophysiol* **78**, 160-9 (1997).
18. Price, J. L. Olfactory system. *in The Human Nervous System (ed. Paxinos, G.) (Academic Press, San Diego)*, 979-1001 (1990).
19. Anderson, A. K. & Phelps, E. A. Is the human amygdala critical for the subjective experience of emotion?: Evidence of intact dispositional affect in patients with amygdala lesions. *Journal of Cognitive Neuroscience* **14**, 709-720 (2002).
20. Robinson, R. G., Kubos, K. L., Starr, L. B., Rao, K. & Price, T. R. Mood disorders in stroke patients. Importance of location of lesion. *Brain* **107 (Pt 1)**, 81-93 (1984).
21. Davidson, R. J. & Irwin, W. The functional neuroanatomy of emotion and affective style. *Trends Cogn Sci* **3**, 11-21 (1999).
22. Bechara, A., Damasio, A. R., Damasio, H. & Anderson, S. W. Insensitivity to future consequences following damage to human prefrontal cortex. *Cognition* **50**, 7-15 (1994).
23. Lazarus, R. J. *Emotion & Adaptation* (Oxford University Press, New York, 1991).
24. O'Doherty, J. et al. Sensory-specific satiety-related olfactory activation of the human orbitofrontal cortex. *Neuroreport* **11**, 893-7 (2000).